REVIEW

Fluid Electrification Measurements of Transformer Pressboard/Oil Insulation in a Couette Charger

A. J. Morin II, M. Zahn, and J. R. Melcher

Massachusetts Institute of Technology
Department of Electrical Engineering and Computer Science
Laboratory for Electromagnetic and Electronic Systems
Cambridge, MA

ABSTRACT

A Couette Charger (CC) facility has been built to simulate flow electrification processes in transformers, where transformer oil fills the annulus between coaxial cylindrical electrodes that can be bare metal or transformer pressboard covered. The inner cylinder can rotate at speeds giving controlled turbulent flow which brings electric charge to the volume from the electrical double layer at the liquid/solid interfaces. This compact apparatus allows for flexibility in testing various oils and transformer pressboards at controlled temperatures and moisture levels in the oil and pressboard. Flow electrification charge density measurements as a function of inner cylinder speed were performed using an absolute charge sensor (ACS). Transient measurements with a step change in temperature have shown the charge density to change from an initial value to a new steady state value, including cases of polarity reversal, both values dependent on the equilibrium moisture levels in oil and pressboard. Through a model that accounts for diffusion of charge from the paper-oil interface into the bulk of the oil, these measurements are used to deduce the equilibrium wall charge density, a parameter which has been found to describe the electrification at all Reynolds numbers. By applying low frequency (0.5 to 4 Hz) high voltages (field strength up to 1.8 kV/cm peak) across the cylinders of the CC the effects of transformer energization are also simulated. To help understand the effects of energization and to scale laboratory measurements at low voltages and low frequencies to operating transformers, a charge injection model was refined to examine the migration of double layer and injected charge in the imposed sinusoidally time varying electric field. Good fits between this model and measurements are achieved with a three parameter estimation of equilibrium charge density at the solid/liquid interface, injected charge density due to energization, and diffusivity in the diffusive sublayer near the wall.

0018-9367 $1.00

1. INTRODUCTION

1.1 BACKGROUND

ELECTRIFICATION has been a past problem in the flow of petroleum liquids in pipes, through filters, and in charge accumulation in storage tanks [1–11]. With changes in the chemical make-up of insulating liquids used to transfer heat and withstand high electric stress, the use of new dielectric materials such as polymers and cellulosic materials, and an increase in the flow speeds for greater cooling, the electrification problem has recently arisen in electric power apparatus [12–24]. Charge separation at interfaces between moving fluid and boundaries with the accumulation of charge on insulators or isolated conductors can lead to high field strengths and electrical discharges. The potential builds up until the rate of charge accumulation equals the rate of charge leakage, or until spark discharges occur. Electrification effects are initiated by fluid flow, whether or not the equipment is energized. Energization usually augments charge separation and exacerbates electrical discharge problems through the insulation. An understanding of electrification requires coupling the laws of electromagnetism, fluid mechanics, heat, and electro-chemistry to describe the four stages of electrification:

1. charge generation,
2. charge transport,
3. charge accumulation, and
4. charge leakage

and to determine how these relate to the observed factors of temperature, moisture, flow rate and turbulence, contaminants and surface active agents, wall surface condition, energization, and flow configuration. What makes understanding difficult is that there is a lack of common denominators in failures. Identical side-by-side transformers have different failure experiences. Trace differences in material properties that are not easily identifiable or controlled, apparently have a strong effect on flow electrification.

1.2 ELECTRIFICATION MEASUREMENT METHODS

There is no standard test procedure for evaluating the charging of flowing dielectric liquids, so that each laboratory has developed their own approach. However, it is important to be aware of artificial effects where flow electrification by the measurement apparatus itself contributes to the measurements. Typical measurement approaches include:

1. Ministatic Tester. This is adapted from electrification measurements in jet fuels to characterize the charge separation process in transformer oils by measuring the electrostatic charging tendency in forcing oil through standard filter paper, a high grade cellulose material chemically similar to transformer paper [25–28]. The oil electrical charging tendency (ECT) is measured by the current from ground necessary to compensate double layer charge entrained in the fluid flow through the filter, or equivalently, measurement of the convection current to the fluid receiver grounded through a low impedance electrometer. The measured current equals the charge density in the oil entering the receiver multiplied by the volume rate of flow through the filter. This apparatus is fast and simple for comparing the relative charging tendencies of different oil samples against a particular material filter. However, it does not seem suited to providing parameters that characterize actual oil-liquid interfaces, especially under operating conditions with energization and/or with transients in temperature, moisture and concentration of other trace materials. The single pass of liquid through the filter does not allow adequate time for the oil and paper to reach moisture or chemical equilibrium.

2. Conducting Probes. A conducting probe placed into the flow results in an open-circuit voltage or short-circuit current but does not provide an unambiguous value of charge density [29] as one may never be certain to the extent to which the probe response is due to impacting charge from the flow, or from charge removed from the probe by the flow by the same charge separation process that is being studied. This objection can also be applied to a charge density probe composed of three equally spaced circular plates [20]. The outer electrodes were grounded and the potential of the floating center electrode was measured by a high-impedance electrometer. Fluid flowing through the probe, even if entering uncharged, will separate some charge from the electrode surfaces, raising the measured potential. There is no way to separate the effects of entering charge due to upstream flow electrification from charge separation within the probe.

3. Isolated Test Pipe Sections. Measurement of the current to an isolated metallic test pipe section gives the difference between the current leaving to that entering [30–32]. Generally, a pipe section simultaneously acts as a relaxation region for entering charge and as a charging region for charge separated within the pipe section. To simulate the transformer duct region, insulating pressboard pipe models have also been used [28]. Measured variables include the streaming current exiting the pipe, leakage currents to conductors or segmented conductors surrounding the pressboard pipe, and the surface potential distribution along the pressboard pipe.

4. Tandem Charge Monitor. Without moving parts, two identical shielded chambers have a dielectric fluid passing through in laminar flow [33]. Each chamber is virtually grounded through electrometers which measure the current to each chamber, from which the charge density in the fluid is computed.

Our work measures the charge density in a fluid dielectric by taking a sample of charged fluid into a Faraday cage to measure the induced image charge via the current from ground required for a short-circuited Faraday cage, or equivalently, measurement of the potential rise of the Faraday cage if it is open circuited. In test pipe measurements, the four electrification stages of charge generation, transport, accumulation, and leakage, spatially overlap, making it difficult to sort out cause and effect. For basic studies, it is desirable to have a flow that is fully developed in both mechanical and electrical senses, which for insulating fluids requires an inconveniently long pipe length.

Our earlier work [34–36] used the Couette Charger (CC) of coaxial cylinders shown in Figure 1 without the absolute charge sensor, but with a small continuous fluid flow to allow charge measurement in the receiver section. The flow path within the CC is closed on itself, so that all parameters must be independent of the azimuthal angle. What appears as a spatial transient in a developing pipe flow appears here as a temporal transient.

Pressure in the fluid reservoir forces the oil through a relaxation chamber (charge trap) so that charge entering the CC is negligibly small. The fluid is charged by the rotation of the inner cylinder and by injection due to applied HV. The charged fluid exits the CC through a shielded metal pipe electrically connected to the receiver tank but insulated from the outer cylinder of the CC by a short length of insulating tube. As charged fluid flows out of the CC into the metal pipe, the convection current is measured by the electrometer connecting the receiver to ground. The electrometer current is the product of the oil charge density and sampling volume rate of flow. With the inner cylinder rotating, the CC isolates the charge generation stage and is a convenient and controllable source of net charge, just as a current source is in an electrical circuit.

The charge density of the fluid is controlled by the rotational speed of the inner cylinder or by the magnitude and frequency of the applied voltage. In our earlier reported work [34–36] charged fluid is delivered at a slow sampling flow rate, independent of the shaft speed as shown in Figure 1. The output current is then measured by summing the currents from the ensuing metal pipe and the receiver. The pipe and metal receiver act as a Faraday cage so that once the charge exits the CC and enters the conducting pipe, it is immediately recorded by the electrometer, whether or not it remains entrained in the fluid or is conducted to the wall by relaxation or mixing. The recorded current also is not affected by charge generation by the flowing fluid within the Faraday cage, as additional charge entrained in the flow is balanced by the image charge remaining on the wall, so that there is no net change in total charge within the Faraday cage.

Central to sorting out electrification processes in the laboratory or in the field, is having an instrument for measuring the net charge density entrained in a liquid. Using the same sampling principles as the CC, the Absolute Charge Sensor also shown in Figure 1 can sample the flow with no net accumulation of fluid independent of the fluid's electrical properties, velocity, and any electrification process within the instrument [37–43]. The ACS periodically transfers a small volume of charged fluid through a shielded sampling probe into an electrically isolated Faraday cage composed of a metal bellows volume driven by a digitally controlled stepper motor. If the fluid is to be returned to the system at a downstream location or to a charge relaxation region, a check valve is used so that the exiting fluid is not in the proximity of the sampling probe. The charge density is calculated from the known filling flow rate and measurement of either the short-circuit current or open-circuit voltage by low or high-impedance electrometers respectively connected to the electrically isolated Faraday cage. For the fluid entering the Faraday cage, streaming currents from flow electrification on the inner surfaces of the probe, check valve, and bellows are not reflected in the measurement as there is no net change in total charge within the ACS.

The system shown in Figure 1 was used simultaneously to measure electrification currents generated by rotation of the inner cylinder by the continuous flow sampling method and with the ACS. On the average, measurements agreed within 1.7% so that the continuous flow measurement approach was no longer used. This allowed the measurement apparatus to be reduced to just the CC and ACS as shown in Figure 2.

1.3 SCOPE OF THIS WORK

The objective here is to measure the fundamental parameters of the flow electrification process that together with the laws of electroquasistatics and physico-chemical hydrodynamics can be used to predict the performance of complex transformer systems. The CC is used because the flow is mechanically and electrically fully developed

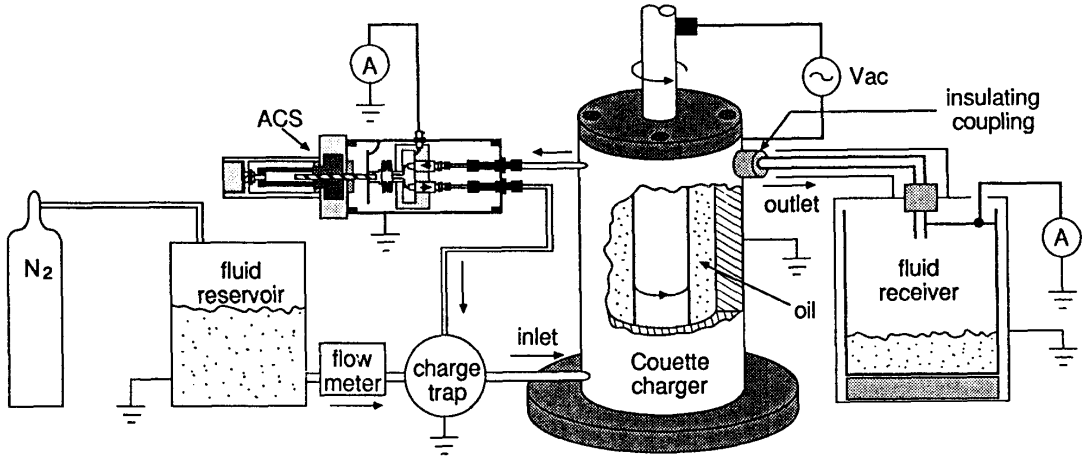

Figure 1.

Couette charging apparatus with the ACS and continuous sampling flow system connected for simultaneous measurements. The outlet metal tube, connected to the CC through an insulating coupling, is electrically connected to the metal fluid receiver to act as a Faraday cage.

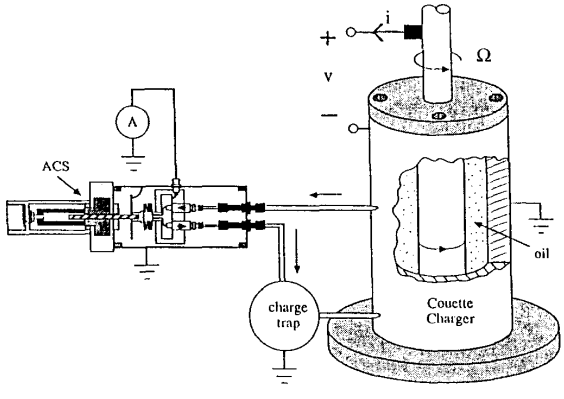

Figure 2.

Couette Charger (CC) with electrical terminals connecting inner and outer cylinders for measuring voltage or current [40] or for applying an ac voltage between the cylinders. The Absolute Charge Sensor (ACS) [38, 43] is used to measure the charge density in the turbulent core.

and has been well studied by hydrodynamicists. All hydrodynamic parameters are set by the rotational velocity of the inner cylinder. Small inventories of oil are used and the wall materials are easily changed. Temperature, applied electrical stress, moisture, and antistatic additives are all easily controllable so that both equilibrium and nonequilibrium conditions can be studied.

The CC annular gap models the cooling ducts in the interwinding regions of a transformer or the coolant tubes of power semiconductor components used in HVDC valves [30–32]. It also models pumps, plenums, and secondary flows due to spacer blocks, protuberances, and bends.

This paper first reviews the critical time scales and characteristic lengths of electrical and mechanical processes in the CC focusing on turbulent fluid mechanics. Using the simplist electrochemical model where the charge density in the electrical double layer ρ_w at the solid/liquid interface wall is fixed, independent of flow velocity, relationships between the measurable variables of charge density ρ_o in the turbulent core the terminal voltage and terminal current are derived from charge conservation relationships and fitted to measurements in the CC with bare metal and paper-covered cylinders by parameter estimating ρ_w for a best fit between the theory and measurements. Measured variables are the charge density in the turbulent core using the ACS, the short-circuit terminal current, and the open-circuit terminal voltage.

Because of the minimum radius allowed for standard treated pressboard, a larger CC facility was also built with improvements for in situ oil impregnation and vacuum drying of the oil/pressboard system to control moisture levels in oil and paper and for control of the operating temperature during measurements. The turbulent core charge density for various transformer oils with bare metal or various pressboard covered cylinders were measured with the ACS during transient step increases and

decreases in temperature for various initial moisture levels in oil and paper. Certain material combinations and operating conditions would result in charge polarity reversal.

Charge density measurements using the ACS were also performed with ac HV applied across the cylinder for various amplitudes and frequencies. The earlier charge injection model used by Lyon *et al.* [34–36] is extended here to also include 'equilibrium' electrical double layer charge that migrates in the electric field across a migration based sub-layer to be entrained in the fully mixed turbulent core. The addition of this charge to the charging current of the turbulent core removes the inconsistency of the earlier Lyon *et al.* analysis which predicted a threshold electric field amplitude before voltage dependent turbulent core charging would occur which was not observed in measurements. With this refined model good fits between turbulent core charge density analysis and data collected for various voltages and frequencies over a wide speed range were obtained by estimating the equilibrium wall charge density ρ_w, the injected charge density due to energization ρ_{inj}, and the diffusivity in the diffusive sub-layer near the wall.

2. THE COUETTE CHARGERS

THE range of speeds at which the inner cylinder can rotate ($\leqslant$ 2000 rpm) in the CC provides the ability to study flows varying from the laminar to fully turbulent regimes, and the symmetry of the experiment enforces uniformity in the circumferential direction, creating a flow that is fully developed in both mechanical and electrical senses.

2.1 MATERIALS USED IN THE COUETTE CHARGER

An important attribute of the Couette system is the relative ease with which it allows for a meaningful examination of different materials: the small inventory of oil can easily be replaced or altered, and the small surface area exposed in the mixer means that different solid materials can be quickly wrapped on the cylinders. The solid insulations tested are representative of those used in transformers and consist primarily of sheets of pressboard and layers of kraft paper.

Two different Couette Chargers were built for our experiments, a small and a large one. The small one of aluminum cylinders was used in experiments [34–36] to examine thin layers of Kraft paper. A larger CC of stainless steel cylinders was required to examine commercial pressboard which for standard fabrication procedures could not be rolled less than 6 inches in diameter to fit over the inner cylinder.

Physical and electric constants of room temperature oil and the dimensions in the two CC units are listed in Table 1 for reference.

Table 1.
Representative room temperature physical and electrical oil parameter values and Couette Charger dimensions.

Parameter	*Symbol*	*Small*	*Large*
Oil permittivity	ε	$2.2\ \varepsilon_o$	
Oil conductivity	σ	10^{-13} to 10^{-10} S/m	
Ion mobility	$b = 2 \times 10^{-11}/\eta$	10^{-9} m^2/(Vs)	
Dynamic viscosity	η	0.02 Ns/m^2	
Kinematic viscosity	$\nu = \eta/\rho_m$	1.8×10^{-5} m^2/s	
Mass density	ρ_m	900 kg/m^3	
Molecular diffusion coefficient	$D_m = bkT/q$	2.5×10^{-11} m^2/s	
Schmidt number	$S = \nu/D_m$	7.2×10^5	
Inner cylinder radius	R_1	2.54 cm	7.62 cm
Outer cylinder radius	R_2	3.81 cm	10.16 cm
Height of Couette Charger	l	22.9 cm	40.64 cm

Pressboards used were EHV-Weidmann T–IV and HIVAL, 0.1 cm thick. They were supplied in a rolled form with the seam left unjoined but prepared for a scarf joint (a gradual tapering on both sides of the seam so that there is no ridge when joined). The pressboard was mounted to the CC cylinders with epoxy and the seam was glued with Imperial Vetak, an oil-compatible white glue supplied by EHV-Weidmann.

The pressboards installed in the CC were generally dried at 90°C for 16 h under a vacuum to remove the moisture that had naturally been absorbed following the drying process used for commercial transformers. Dry oil was then added to the CC while still under vacuum to oil-impregnate the pressboard.

2.2 CRITICAL PARAMETERS

2.2.1 CHARACTERISTIC TIMES

Certain time constants associated with electrification phenomena help explain the transients evident in measurements. These are described below and listed in Table 2 including typical values in the CC units:

Table 2.
Characteristic room temperature electrical and fluid mechanical time constants in the Couette systems.

Time	*Formula*	*Typical Values in Small Couette System*	*Typical Values in Large Couette System*
Self-precipitation Time	$\tau_p = \frac{\varepsilon}{\rho b}$	6500 – 130 s for $\rho = 3 - 150\ \mu C/m^3$	
Relaxation Time	$\tau_e = \frac{\varepsilon}{\sigma}$	200 – 0.2 s with $\sigma = 10^{-13} - 10^{-10}$ S/m	
Molecular Diffusion Time	$\tau_d = \frac{\delta d}{2D_m}$	3429 s for 1000 rpm ($R = 2800, \delta = 13.5\ \mu m$)	3886 s for 1000 rpm ($R = 15000, \delta = 7.7\ \mu m$)
Turbulent Development Time	$\tau_{dev} = \frac{d^2}{D_T}$	1.20 – 0.47 s for 500 – 1800 rpm or $R = 1400 - 5040$	1.4 – 0.53 s for 500 – 1800 rpm or $R = 7500 - 27000$

Self-precipitation time

The self-precipitation time τ_p of charge with density ρ and mobility b is

$$\tau_p = \frac{\varepsilon}{\rho b} \tag{1}$$

where the mobility is estimated using an empirical rule (in SI units) for positive ions in insulating dielectrics with absolute viscosity η [44]:

$$b \approx \frac{2 \times 10^{-11}}{\eta}\ \mathrm{m^2/(Vs)} \tag{2}$$

For our transformer oils at 21°C, $\eta = 20$ cp $= .020$ N s/m^2 so that $b \approx 10^{-9}$ m^2/(Vs). Typical measured charge densities in transformers vary over the wide range of 1 to 1000 μC/m^3 so that the self-precipitation time varies from 19000 down to 19 s; however, the measured charge densities in our CC experiments are more on the order of 3 to 150 μC/m^3, indicating large self-precipitation times of 6500 down to 130 s. Because of this generally small charge density, this time is typically much longer than the dielectric relaxation time so we can ignore it. This can be equivalently stated that the ohmic conductivity $\sigma \gg \rho b$.

Dielectric relaxation time, τ_e

The dielectric relaxation time τ_e, given by

$$\tau_e = \frac{\varepsilon}{\sigma} \tag{3}$$

can vary by orders of magnitude because of the large variation in ohmic conductivity of insulating oils as a function of parameters not easily controlled. The permittivity of our oils have approximately the constant value of $\varepsilon = 2.2\varepsilon_o$ but have ohmic conductivities ranging from $\sigma = 10^{-13}$ to 10^{-10} S/m yielding relaxation times of 200 to 0.2 s. This large range of conductivity is due to contamination of the oil from the pressboard and changes in temperature. By raising the temperature from 35 to 70°C, the oil conductivity increases approximately by a factor of five. In our experiments, we have found that operation with T–IV pressboard increases the oil conductivity by as much as a factor of one hundred whereas HIVAL increases it by as much as a factor of five. Trace ionizable materials are evidently being transferred from the pressboard to the oil during the experiments.

Molecular diffusion time τ_d

The molecular diffusion time is the time it takes charge with diffusivity D_m to diffuse across a sublayer of thickness δ in a gap of thickness d

$$\tau_d = \frac{\delta d}{2D_m} \tag{4}$$

where $d = R_2 - R_1$ is the gap spacing between inner and outer cylinders.

Turbulent development time τ_{dev}

As a first-order approximation to the time required for the turbulent flow in the Couette Charger to develop, we calculate a diffusion time using the coefficient of turbulent diffusion D_T:

$$\tau_{dev} \approx \frac{d^2}{D_T} \tag{5}$$

This time is generally short compared to other system time constants because D_T greatly exceeds D_m due to the turbulent mixing processes.

2.2.2 TURBULENT FLUID MECHANICS

As the flow velocity is increased, in addition to a mean flow, the flow profile has rapidly varying fluctuations in time and space. These velocities fluctuate about a mean value with variations generally large compared to the mean value. The fluid paths are extremely complicated resulting in extensive mixing. The flow profile separates into three regions: a wall sublayer with steep velocity gradient and main turbulent outer layer joined by an overlap transition layer [45a]. The wall sublayer has sometimes been called a laminar sublayer, because the mean flow profile obeys the laminar flow equations with kinematic viscosity $\nu = \eta/\rho_m$ (m^2/s), where ρ_m is the fluid mass density, but this is a misnomer as turbulent fluctuations are present right up to the wall [46]. In the turbulent flow region the viscosity ν is replaced by an enhanced eddy viscosity ν_T which accounts for the great mixing due to the turbulent fluctuations. The exact flow profile for turbulent flow is not amenable to theoretical description, so analysis relies on empirical measurements and dimensional analysis in terms of the friction velocity

$$v^* = \sqrt{\frac{\tau_w}{\rho_m}} \tag{6}$$

where τ_w is the wall shear stress. The wall law gives the mean shear velocity near the wall to first vary linearly with distance x from the wall [45a]

$$\frac{v_z}{v^*} = \frac{xv^*}{\nu} \qquad 0 \le \frac{xv^*}{\nu} < 5 \tag{7}$$

This velocity profile merges in the transition overlap layer to the logarithmic overlap law

$$\frac{v_z}{v^*} = \frac{1}{\chi}\ln\left(\frac{xv^*}{\nu}\right) + 5 \qquad \frac{xv^*}{\nu} > 30 \tag{8}$$

where $\chi \approx 0.41$ is called the von Karman mixing-length constant. Because the fluctuating velocity components are exactly zero at the wall, a Taylor series expansion of the second moment fluctuations near the wall together with empirical measurements for numerical coefficients give [46]

$$\begin{aligned}
\left[\frac{\overline{v_z'^2}}{v^{*2}}\right]^{1/2} &\approx 0.3\frac{xv^*}{\nu} \\
\left[\frac{\overline{v_y'^2}}{v^{*2}}\right]^{1/2} &\approx 0.07\frac{xv^*}{\nu} \\
\left[\frac{\overline{v_x'^2}}{v^{*2}}\right]^{1/2} &\approx 0.008\left(\frac{xv^*}{\nu}\right)^2 \\
\left[-\frac{\overline{v_z'v_x'}}{v^{*2}}\right] &\approx 0.001\left(\frac{xv^*}{\nu}\right)^3
\end{aligned} \tag{9}$$

The result of this turbulent mixing is to enhance the fluid kinematic viscosity from ν to the eddy viscosity ν_T and the molecular diffusivity D_m to the eddy diffusivity D_T where ν_T and D_T vary with position from the wall. Turbulent fluid motions that enhance momentum transfer also enhance heat, mass, and charge transfer in the same way, known as Reynolds' analogy. For our case, this requires that $D_T \approx \nu_T$. Using (7) and $[\overline{v_z'v_x'}]$ in (9) the turbulent kinematic viscosity increases cubically with distance x from the wall

$$\frac{\nu_T}{\nu} = -\frac{\overline{v_z'v_x'}}{\nu\,\partial v_z/\partial x} \approx 0.001\left(\frac{xv^*}{\nu}\right)^3 \tag{10}$$

Empirical measurements provide the turbulent viscosity dependence on distance farther away from the wall. Using a mathematical fit that approaches (10) as $x \to 0$ gives ν_T/ν as a function of distance x from the wall for a pipe as [47–49]

$$\left(\frac{\nu_T}{\nu}\right)_{\text{pipe}} \approx 0.4\left[\frac{xv^*}{\nu} - 11\tanh\left(\frac{xv^*}{11\nu}\right)\right] \tag{11}$$

which is approximately valid up to one quarter of the pipe radius from the wall. For planar Couette flow of channel depth d with linear velocity profile from zero at the wall [47, 48]

$$\left(\frac{\nu_T}{\nu}\right)_{\text{Couette}} = \frac{(\nu_T/\nu)_{\text{pipe}}}{1 + 1.72(x/d)^3} \tag{12}$$

In the highly mixed turbulent core out to approximately 3/4 of the radius, $D_T \approx \nu_T$ becomes approximately constant

$$D_T \approx 0.1v^*d \tag{13}$$

The friction velocity of (6) can be computed with empirical correlations for particular flow geometries. G. I. Taylor has correlated the normalized wall stress at the stationary outer cylinder for Couette flow [50]

$$\frac{\tau_w}{\rho_m(\Omega R_2)^2} \approx 0.1R^{-1/2} \qquad 300 \le R \le 10000 \tag{14}$$

in terms of the angular velocity Ω (rad/s) of the inner cylinder, the outer cylinder radius R_2, and the fluid Reynolds number R. Using the oil viscosity and CC geometries in Table 1, the Reynolds number for Couette flow,

$$R = \frac{\Omega R_2 d}{\nu} \tag{15}$$

at room temperature is 2.8× the rotational speed in RPM for the small CC and 15.0× the rotational speed for the large. From (14) in (6)

$$v^* = 0.32\frac{\nu}{d}R^{3/4} \tag{16}$$

From (13), the core turbulent diffusion coefficient depends on Reynolds' number as

$$D_T = 3.2 \times 10^{-2}\nu R^{3/4} \tag{17}$$

Thus for our oil viscosity of $\nu = 1.8 \times 10^{-5}$ m^2/s ($\rho_m = 900$ kg/m^3) and at a rotational speed of 1000 rpm, the Reynolds number in the small CC is 2800 which gives a turbulent diffusion coefficient of $D_T = 2.2 \times 10^{-4}$ m^2/s and a turbulent development time of $\tau_{dev} = 0.73$ s. In the large CC with a rotational speed of 1000 rpm, the Reynolds number is 15, 000 which gives $D_T = 7.8 \times 10^{-4}$ m^2/s and $\tau_{dev} = 0.83$ s. Thus within the second that the inner cylinder has reached a steady speed of 1000 rpm, the core for either CC is fully mixed and turbulent.

2.2.3 CHARACTERISTIC LENGTH SCALES

Because of the spatial dependence of turbulent fluid flow, there are several important electrical and hydrodynamic length scales. These lengths are summarized in Table 3, which includes typical values of each parameter in our CC systems.

Debye length, λ

The stagnant Debye length results from a balance of the ion diffusion time, λ^2/D_m, with the relaxation time, ϵ/σ:

$$\lambda = \sqrt{\frac{\epsilon D_m}{\sigma}} = \sqrt{D_m \tau_e} \tag{18}$$

The molecular diffusion coefficient D_m is related to charge mobility by the Einstein relation:

$$\frac{D_m}{b} = \frac{kT}{q} \approx 25 \text{ mV} \tag{19}$$

so that at room temperature our mobility $b \approx 10^{-9}$ m^2/(Vs) yields $D_m \approx 2.5 \times 10^{-11}$ m^2/s. For our conductivity range of 10^{-13} to 10^{-10} S/m, the Debye length then ranges approximately from 70 to 2.2 μm.

Turbulent Debye length, λ_T

If the double layer extends past the diffusion sublayer into the turbulent core, the mixing uniformly disperses the charge over a thickness given by the turbulent Debye length described by the turbulent diffusion coefficient D_T.

$$\lambda_T = \sqrt{\frac{\epsilon D_T}{\sigma}} \tag{20}$$

Using (17) the conductivity range of 10^{-13} to 10^{-10} S/m yields a turbulent Debye length from approximately 210 mm to 6.6 mm for a rotational speed of 1000 rpm in the small CC. In the large CC with a rotational speed of 1000 rpm, the turbulent Debye length ranges approximately from 390 to 12 mm. For most of our measurements $\lambda_T > d$ so that the core is fully mixed.

Viscous sublayer thickness, δ_v

As the simplest approximation for electrification phenomena, we divide the turbulent flow profile into two regions, a wall viscous sublayer with mean flow described by laminar flow equations, and a turbulent core. The thickness of the viscous sublayer is that distance from the wall $x = \delta_v$ where $\nu_T/\nu \approx 1$. The exact numerical coefficient is picked to best fit measurements so that [45a, 51]

$$\delta_v = \frac{5\nu}{v^*} \tag{21}$$

which becomes

$$\delta_v = 15.6 d R^{-3/4} \tag{22}$$

which is 515 μm for the small CC and 292 μm for the large CC at 1000 rpm.

Diffusion sublayer thickness, δ_d

The thickness of the diffusion sublayer is similarly defined as that distance where $D_T/D_m \approx \nu_T/D_m \approx 1$, again choosing the numerical coefficient from best fits to empirical measurements [49, 52]

$$\delta_d = \frac{11.7\nu}{S^{1/3} v^*} = \frac{36.5 d R^{-3/4}}{S^{1/3}} \qquad S = \frac{\nu}{D_m} \tag{23}$$

which is 13.6 μm for the small CC and 7.7 μm for the large CC at 1000 rpm.

These thicknesses differ by factors of the Schmidt number S which generally greatly exceeds unity. Thus for usual dielectric liquids the Schmidt number is large so that $\delta_d < \delta_v$. Within the viscous sublayer, the kinematic viscosity is taken to be ν while outside the sublayer the kinematic viscosity is $\nu_T = D_T$ given by (11), (12) or (13). Within the diffusive sublayer the diffusivity is given by the molecular diffusion coefficient D_m, while outside the sublayer the diffusivity is given by $D_T = \nu_T$.

Migration length, δ_{mig}

The maximum distance that charge can migrate in an ac electric field with amplitude E_o and frequency ω is

$$\delta_{mig} = 2bE_o/\omega \tag{24}$$

This length is important for energization charging where the electric field drives the electrical double layer charge into the strongly mixed turbulent core.

Table 3.
Characteristic room temperature electrical and fluid mechanical lengths in the Couette systems.

Length	*Formula*	*Typical Values in Small Couette System*	*Typical Values in Large Couette System*
Debye Length	$\lambda = \sqrt{\frac{\varepsilon D_m}{\sigma}}$	70 – 2.2 μm for $\sigma = 10^{-13} - 10^{-10}$ S/m $D_m = 2.5 \times 10^{-11}$ m²/s	
Turbulent Debye Length	$\lambda_T = \sqrt{\frac{\varepsilon D_T}{\sigma}}$	210 – 6.6 mm at 1000 rpm $\sigma = 10^{-13} - 10^{-10}$ S/m $D_T = 2.2 \times 10^{-4}$ m²/s	390 – 12 mm at 1000 rpm $\sigma = 10^{-13} - 10^{-10}$ S/m $D_T = 7.8 \times 10^{-4}$ m²/s
Viscous Sub-Layer Thickness	$\delta_v = \frac{5\nu}{\sqrt{\tau_w/\rho_m}} = 15.6dR^{-3/4}$	866 – 331 μm for 500 – 1800 RPM (d = 12.7 mm)	492 – 188 μm for 500 – 1800 RPM (d = 25.4 mm)
Diffusion Sub-Layer Thickness	$\delta_d = \frac{11.7\nu}{S^{1/3}\sqrt{\tau_w/\rho_m}} = 36.5dR^{-3/4}/S^{1/3}$	22 – 9 μm for 500 – 1800 RPM	13 – 5 μm for 500 – 1800 RPM
Migration Length	$\delta_{mig} = 2bE_o/\omega$	159 μm for $E_o = 0.5 \times 10^6$ V/m and $\omega/2\pi = 1$ Hz	
Migration Sublayer Thickness	$\delta_b = 63dR^{-9/8}[bE_o d/\nu]^{1/2}$	63μm for $E_o = 0.5 \times 10^6$ V/m and 1000 rpm	27 μm for $E_o = 0.5 \times 10^6$ V/m and 1000 rpm

Migration sub-layer thickness, δ_b

Charge within the electrical double layer will migrate in an electric field of amplitude E_o with a velocity bE_o. The charge migration sublayer thickness is defined as that distance from the wall when the peak migration velocity just equals the fluid fluctuation rms velocity component perpendicular to the wall $(\overline{v_x'^2})^{1/2}$ given in (9)

$$bE_o = \sqrt{\overline{v_x'^2}} = 0.008(\frac{\delta_b}{\nu})^2(\frac{\tau_w}{\rho_m})^{3/2} = 2.53 \times 10^{-4}\delta_b^2\nu R^{9/4}/d^3 \quad (25)$$

Migrating charge which crosses this sublayer becomes entrained into the turbulent core flow.

2.3 COUETTE FLUID MECHANICS

2.3.1 FLOW REGIMES

The flow distributions in the CC with the inner cylinder rotating have three regimes: laminar, cellular convection, and turbulent. The rotational speeds for each of these regimes for both the small and large CC are approximately calculated from the Taylor number [45b, pp. 423–426] T_a for a small gap:

$$T_a = \frac{R_1 d^3 \Omega^2}{\nu^2} \quad (26)$$

Laminar flow

Applies to low rotational speeds such that $T_a < 1708$, with no radial velocity component. (Small CC, $\Omega <$ 31 rpm; Large CC, $\Omega < 6$ rpm).

Cellular convection

As the speed passes through a (relatively low) critical value, the flow experiences a type of instability not found in pipe flows: the smooth laminar flow breaks up into three-dimensional convection cells. This occurs for Taylor numbers $1708 < T_a < 160000$. (Small CC, 31 rpm< Ω <301 rpm; Large CC, 6 rpm< Ω <62 rpm).

Turbulence

As the rotational speed increases past the critical value, the cells begin to break up and eventually give way to fully developed turbulent flow. This occurs for Taylor numbers $T_a > 160000$. (Small CC, $\Omega > 301$ rpm; Large CC, $\Omega > 62$ rpm).

2.3.2 TURBULENT FLOW

With steady rotational speed, the torques on the inner and outer cylinders of length l are equal and related to

the wall shear stresses τ_{w1} and τ_{w2} at the oil/cylinder interfaces and respective radii R_1 and R_2 by

$$Torque = \tau_{w1} 2\pi R_1^2 l = \tau_{w2} 2\pi R_2^2 l \tag{27}$$

With a fully developed turbulent flow, the diffusion sublayer thicknesses $\delta_{1,2}$ [49,52] at these interfaces are related to the wall shear stresses $\tau_{w1,2}$, mass density ρ_m, molecular diffusion coefficient D_m, and kinematic viscosity ν by

$$\delta_{1,2} = \frac{11.7\nu}{S^{1/3}\sqrt{\tau_{w1,2}/\rho_m}} \tag{28}$$

Since from (27) the wall shear stresses are in inverse proportion to the square of the radii, (28) shows that the diffusion sub-layer thicknesses are in direct proportion to the cylinder radii, $\delta_1/\delta_2 = R_1/R_2$. The Taylor correlation (14) [50] relates the wall shear stress at the stationary outer cylinder to the inner cylinder rotational velocity Ω by

$$\tau_{w2} = \tau_{w1}(\frac{R_1}{R_2})^2 = 0.1\rho_m(\Omega R_2)^{3/2}\left(\frac{\nu}{d}\right)^{1/2} \tag{29}$$

2.4 CHARGE CONSERVATION

A wall volume charge density ρ_w is used to describe the governing electrokinetics in the CC at the oil/cylinder interface. It can be inferred from ACS measurements of the core charge density ρ_o.

Conservation of charge

$$\oint_S \bar{J}\cdot\bar{n}\,da = -\frac{d}{dt}\int_V \rho\,dV$$
$$\bar{J} = \bar{J}_d + \sigma\bar{E} = -D\nabla\rho + \sigma\bar{E} \tag{30}$$

with current density due to diffusion and ohmic conduction is applied to a closed surface S as shown in Figure 3a which contains the volume $V = \pi(R_2^2 - R_1^2)l$ of oil between the cylinders. Because δ_1 and δ_2 are typically much smaller than R_1, the volume of the fully mixed turbulent core where the charge density is assumed to be uniform is approximately the same. A linear profile as shown in Figure 3b of the charge density over the sub-layer thickness is assumed so that (30) yields

$$V\frac{d\rho_o}{dt} = 2\pi l(J_{d1}R_1 + J_{d2}R_2) - V\rho_o\sigma/\varepsilon$$
$$J_{d1,2} = (\rho_{w1,2} - \rho_o)D/\delta_{1,2} \tag{31}$$

where The last term on the right of (31) comes from Gauss' law which requires that the flux of displacement field through the closed surface to equal the total volume charge.

$$\oint_S \bar{E}\cdot\bar{n}\,da = \int \frac{\rho\,dV}{\epsilon} \tag{32}$$

In the large CC with radii $R_1 = 7.62$cm and $R_2 = 10.16$cm, length $l = 40.64$cm, oil conductivity $\sigma \approx 10^{-12}$ S/m, permittivity $\epsilon = 2.2\epsilon_o$, mass density $\rho_m = 900\,\mathrm{kg/m^3}$, kinematic viscosity $\nu = 1.8\times10^{-5}\,\mathrm{m^2/s}$, and molecular diffusion coefficient $D_m = 2.5\times10^{-11}\,\mathrm{m^2/s}$, the Debye length $\lambda = (\varepsilon D_m/\sigma)^{1/2}$ is 22 μm and the diffusion sublayer thickness decreases from 43 to 5 μm as the speed is increased from 100 to 1800 rpm. The assumption of a linear profile over the sub-layer is somewhat approximate because the Debye length is less than the sub-layer thickness over the low speed ranges. But for speeds > 247 rpm, where the Debye and sublayer lengths are equal, this approximation will give results close to those of more complete analysis. The charge density in the turbulent core is essentially uniform due to the great mixing because the turbulent Debye length $\lambda_T = (\varepsilon D_T/\sigma)^{1/2}$ with turbulent diffusion coefficient $D_T = 3.2\times10^{-2}\nu R^{3/4}$ ranges from 5.2 to 15.3 cm which is greater than the gap thickness between the cylinders of 2.54 cm.

Reducing (31), the governing equation for the core charge density is related to the wall charge densities $\rho_{w1,2}$, diffusion times $\tau_{d1,2}$, and dielectric relaxation time τ_e by

$$\frac{d\rho_o}{dt} + \left(\frac{1}{\tau_{d1}} + \frac{1}{\tau_{d2}} + \frac{1}{\tau_e}\right)\rho_o = \frac{\rho_{w1}}{\tau_{d1}} + \frac{\rho_{w2}}{\tau_{d2}}$$
$$\tau_{d1,2} \equiv \tau_d = \frac{\delta_{1,2}(R_2^2 - R_1^2)}{2DR_{1,2}} \tag{33}$$
$$\tau_e = \frac{\varepsilon}{\sigma}$$

where The diffusion times at the inner and outer cylinders are equal because the sublayer thicknesses $\delta_{1,2}$, are in direct proportion to the radii $R_{1,2}$. In our experiments the inner and outer cylinder walls were covered with the same materials so in continuing analysis we will take the wall charge densities at inner and outer cylinders to be equal, $\rho_{w1} = \rho_{w2} \equiv \rho_w$.

2.5 TERMINAL VOLTAGE AND CURRENT

The core charge density ρ_o and coaxial cylindrical geometry also gives rise to a short-circuit current or open-circuit voltage in the external circuit connecting inner and outer cylinders [40].

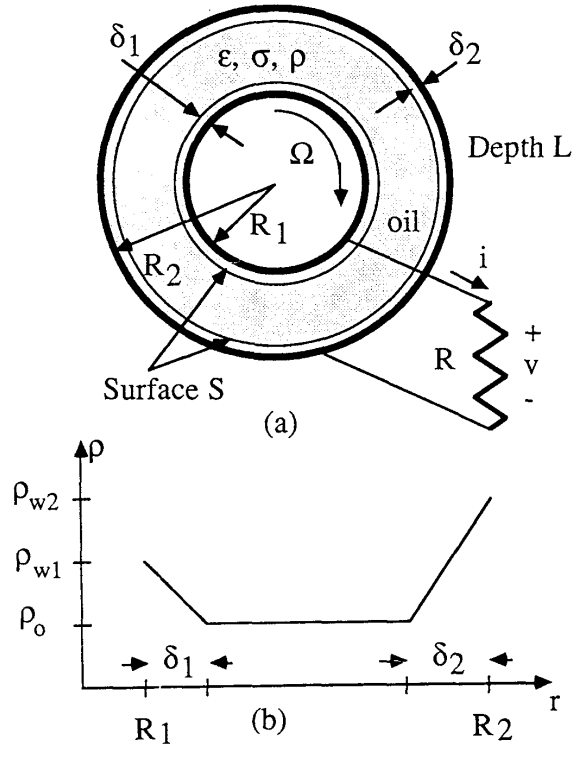

Figure 3.

(a) Cross section of the Couette Charger with load resistance R connected to the terminals. (b) Charge density distribution between the inner and outer cylinders showing the wall charge densities ρ_{w1} and ρ_{w2} which describe the governing electrokinetics at the oil/cylinder interfaces. Also shown is the linear charge density profiles in each sublayer joining the wall charge density values to the turbulent core charge density ρ_o at the edge of each sublayer.

The electric field distribution between the cylinders is related to the terminal voltage v, radial position r, and core charge density ρ_o by

$$\bar{E} = \bar{i_r}\left[\frac{\rho_o r}{2\varepsilon} + \frac{v - \rho_o(R_2^2 - R_1^2)/4\epsilon}{r\ln(R_2/R_1)}\right] \tag{34}$$

Again using conservation of charge, the terminal current may be evaluated by summing the current densities at either the inner or the outer cylinder which will result in the same expression. The current (evaluated at the inner cylinder) is the sum of the ohmic, diffusion, and displacement current densities multiplied by the area of the cylinder.

$$i = -\left[\sigma E_1 + \frac{D}{\delta_1}(\rho_{w1} - \rho_o) + \varepsilon\frac{dE_1}{dt}\right] 2\pi R_1 l \tag{35}$$

where $E(r = R_1) = E_1$ is the electric field at the inner cylinder. Substitution of (34) evaluated at the inner cylinder ($r = R_1$) into (35), using (33) to relate the time derivative of ρ_o to ρ_o and the wall charge densities, together with the resistive terminal constraint ($v = iR$) gives the terminal voltage as

$$C\frac{dv}{dt} + \left[\frac{1}{R} + \frac{1}{R_{int}}\right]v = \frac{(\rho_w - \rho_o)V}{\tau_d}\left[\frac{R_2^2 + R_1^2}{R_2^2 - R_1^2} - \frac{1}{ln(R_2/R_1)}\right] \tag{36}$$

where C is the capacitance and R_{int} is the resistance between cylinders

$$\frac{C}{\varepsilon} = \frac{1}{\sigma R_{int}} = \frac{2\pi l}{\ln(R_2/R_1)} \tag{37}$$

The steady state solution of (33) for the core charge density is

$$\rho_o = \frac{\rho_w}{1 + \tau_d/2\tau_e} \tag{38}$$

If the inner cylinder has been rotating at constant speed for a long time such that ρ_o has reached constant value, (38) shows that the turbulent core charge density is independent of the terminal loading between cylinders. In preliminary measurements using the ACS, ρ_o was found to have a negligible dependence on terminal resistance, decreasing $< 1\%$ when the terminals were switched from open to short circuit. When the charge density is in the steady state, (38) allows us to eliminate ρ_w in favor of the measured charge density ρ_o.

With the turbulent core charge density in the steady state, given by (38) and with a high-impedance electrometer ($R \to \infty$) connected to the terminals of the Couette Charger, (36) then reduces to a differential equation which relates the terminal open-circuit voltage to the steady state core charge density

$$\frac{dv_{oc}}{dt} + \frac{v_{oc}}{\tau_e} = -\frac{\rho_o}{4\varepsilon\tau_e}\left[(R_1^2 + R_2^2)\ln(R_2/R_1) - (R_2^2 - R_1^2)\right] \tag{39}$$

With a low-impedance electrometer ($R \to 0$), (36) with (38) and $i = v/R$ reduces to an equation which relates the terminal short-circuit current to the core charge density

$$i = \frac{-\rho_o \pi l}{2\tau_e \ln(R_2/R_1)}\left[(R_2^2 + R_1^2)\ln(R_2/R_1) - (R_2^2 - R_1^2)\right] \tag{40}$$

The short-circuit current responds instantaneously as open circuited terminals are short circuited, while the reverse process (where short-circuited terminals are open

circuited) has a time constant of τ_e for the voltage to reach steady state. The ratio of steady state open-circuit voltage to short-circuit current is just R_{int}. For the polarity convention chosen, as shown in Figures 2 and 3, a positive core charge density will have an open-circuit voltage and short-circuit current that are negative.

Although there is no mean flow in the direction of the generated radial electric field, there are fluctuating velocity components in the radial direction so that the terminal current delivers a small amount of power to a resistive load connected between the cylinders. These measurements and analysis illustrate how turbulent diffusion can do work and hence be the mechanism for mechanical to electrical energy conversion.

3. UNENERGIZED CHARGING MEASUREMENTS

MEASUREMENTS of the core charge density ρ_o and terminal current or voltage have been taken in both CC for a variety of oils and materials covering the cylinders. Some of the data was taken with a step change in temperature to examine the effects of moisture dynamics between oil and pressboard. All data were taken with the ACS probe at half the height of the CC to minimize end effects from the CC top and bottom. To examine the spatial uniformity of the core charge density, initial ACS measurements were made with bare aluminum cylinders in the small CC with the probe tip moved radially from the outer wall to gap center. Measurements showed that the charge density spatial distribution was essentially uniform for inner cylinder rotational speeds above 400 rpm. For all subsequent measurements in either CC the probe was placed flush with the inner surface of the outer cylinder when bare metal cylinders were tested. With pressboard covered cylinders, the probe was placed flush with the inner surface of the pressboard on the outer cylinder. This position minimizes the probe effect on the flow and reduces the electric field at the probe tip when ac voltages are applied.

3.1 DIELECTRIC RELAXATION MEASUREMENTS

The dielectric relaxation times τ_e to be reported were the measured time constants of the open-circuit voltage decay when a 22 V battery was disconnected from the terminals of the CC without rotation as shown in Figure 4. For a representative measurement of new Shell oil, the conductivity for a measured dielectric relaxation time of $\tau_e = 38$ s is $\sigma = 0.51$ pS/m.

This measurement with Shell oil was initially checked by the following additional methods: [39, 42]

1. Measurement of resistance between cylinders using an electrometer in resistance measurement mode and then calculating the ohmic conductivity. For the test sample in the small CC, this measurement gave $\sigma = 0.75$ pS/m.
2. Measurement of dc resistance R and capacitance C of an open parallel plate capacitor submerged into the oil and calculating the relaxation time from

$$\tau_e = RC \tag{41}$$

   For the initial test sample this method gave an oil conductivity of $\sigma = 0.88$ pS/m.
3. Measurement of the open-circuit relaxation time when the submerged parallel plate capacitor is initially charged and then open circuited. For the test sample the oil conductivity by this method was $\sigma = 0.59$ pS/m.
4. Impedance measurement of magnitude and angle at 0.1 Hz across the plates of the submerged capacitor. This measurement gave $\sigma = 0.97$ pS/m and $\epsilon/\epsilon_o = 2.2$.

As often occurs for such highly insulating liquids, different measurement methods give slightly different conductivity values. We chose the open-circuit voltage decay time constant method as illustrated in Figure 4 as our standard method for measurement of the dielectric relaxation time. The open-circuit voltage decay method was also used for pressboard-covered cylinders because the thin oil-impregnated pressboard had series resistance much less than the thicker oil gap.

3.2 MEASUREMENTS IN THE SMALL CC WITH BTA

Japanese researchers report a reduction in charging tendency with the use of 10 ppm BTA (1, 2, 3-Benzotriazole) in transformer oil [28], but this antistatic effect has not been observed by U. S. researchers [25–27]. Ieda *et al.* [53] report that the addition of 50 ppm BTA reduced the charge density of ~ 3.2 to ~ 0.3 μC/m^3. In our preliminary studies on the effects of BTA on the charging tendency in the small CC with Manning-220 paper-covered cylinders, we found that core charge densities decreased only by about 30% with the addition of 50 ppm BTA [39, 42]. However, the Japanese investigators believe that the beneficial effect of BTA on reducing the electrification hazard is due to suppression of the oxidative degradation of copper and long-term (many months to years) selective adsorption of BTA to paper. In our experiments there was no copper, just the aluminum cylinders of the small CC, and the BTA was in the oil/paper system for

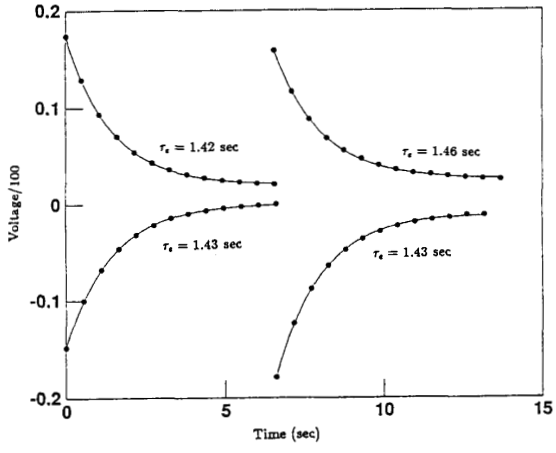

Figure 4.

Representative dielectric relaxation time measurement (Entry 8 in Table 6). A 22 V source was disconnected from the CC terminals and the open-circuit voltage decay was recorded. This was done twice and then the source was reversed in polarity and the measurement repeated. The time constant was estimated for each response and then an average was taken.

only 31 days. Future work will place a copper sleeve between the stainless steel cylinders of the large CC and pressboard covering. Transformer oil with BTA additive will contact the copper/pressboard cylinder coverings for long enough time to see if BTA has a beneficial effect in reducing electrification processes.

3.2.1 TEMPORAL TRANSIENT MEASUREMENTS

Gulf Transcrest H oil with 50 ppm BTA in contact with Manning-220 paper was used for terminal measurement experiments. With the terminals of the small Couette Charger (shown in Figure 2) connected to a low impedance electrometer, the short-circuit current was measured as shown in Figure 5. A negative current was measured which increased in magnitude with increasing speed. Figure 6. shows the transient response of the negative terminal voltage when switched from an initial short-circuit condition to an open circuit at $t = 0$. For each value of rotational speed, the speed was held constant for at least 5 min before the terminals were opened so that the core charge density was at its steady state value. For each speed, the voltage magnitude increased exponentially with a measured time constant of 43 s. From (39), this time constant should be the dielectric relaxation time of the oil which was estimated by two different methods to be $\tau_e \approx 30$ s. One of the methods was a dc resistance measurement, using a Keithley 616 electrometer, across an open parallel plate capacitor submerged in the oil. The other measured the time constant of the open-circuit voltage decay when a 22 V battery was disconnected from the terminals of the CC without rotation as in Figure 4. Both methods gave approximately the same value of conductivity which was $\sigma \approx 6 \times 10^{-13}$S/m. Using $\varepsilon = 2.2\varepsilon_o$, this gives a dielectric relaxation time of $\tau_e \approx 30$ s, somewhat lower than the measured 43 s charging time constant in Figure 6. Also shown in Figure 6 is the unexplained much faster open-circuit voltage decay after rotation of the inner cylinder was stopped. Since the turbulent development time is short, the turbulent flow in the gap between the cylinders will quickly settle when the rotation is stopped. With essentially no flow in the CC, $\delta_{1,2}$ become large so that the diffusion times become so large that all diffusion time terms in (33) become negligibly small. The charge density then decreases as $\rho_o = \rho_{oo} \exp(-t/\tau_e)$ after the rotation is stopped where ρ_{oo} is the initial charge density value equal to the steady state charge density of (38) when the cylinder is rotating. With the right hand side of (36) negligibly small, the open-circuit voltage ($R \to \infty$) then should decay from its initial value to zero with dielectric relaxation time constant τ_e. Possible reasons for the disagreement in measured time constants for charging and decay from the model are discussed in Section 3.2.3.

3.2.2 STEADY STATE MEASUREMENTS

Using the ACS, the steady state turbulent core charge density ρ_o was also measured as a function of inner cylinder rotational speed as shown in Figure 7. Simultaneously measured were the short-circuit current or open-circuit voltage across the terminals of the charger. Using (39) and (40) in the steady state, the fully mixed turbulent core charge density was calculated from the measured steady state open-circuit voltage and short-circuit current which are also shown in Figure 7. Fitting the wall charge density to $\rho_w \approx 740\ \mu$C/m^3 so that (38) (with $\tau_e = 30$ s.) agreed with the ACS measured charge density value at 1800 rpm, (38) was plotted as a function of rotational speed to have excellent correlation with the other charge density values measured by the ACS at lower speeds.

The measured short-circuit current gave core charge densities about 3 to 4× greater than those measured from the ACS. The correlation from the measured open-circuit voltage was slightly better.

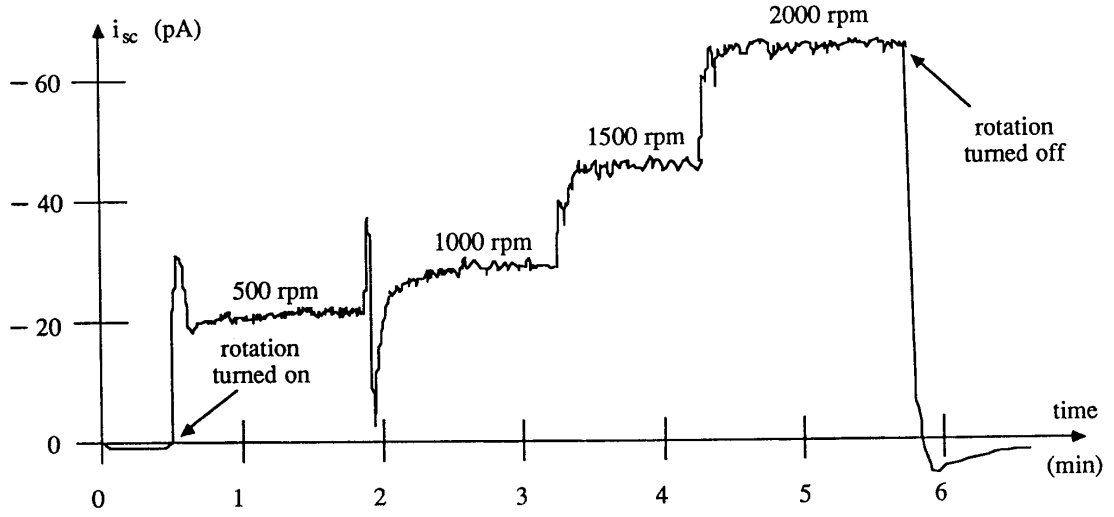

Figure 5.

Measured (negative) short-circuit current as a function of time in the small CC with the rotational speed changed from 0 to 2000 rpm in steps of 500 rpm.

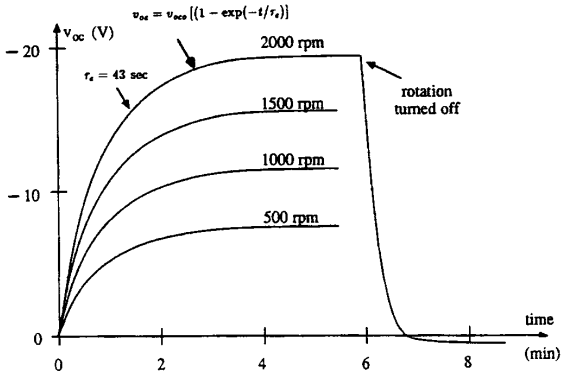

Figure 6.

Measured (negative) open-circuit voltage transient response from an initial short circuit for different rotational speeds in the small CC. A dielectric relaxation time of 43 s would give good agreement between the measurements and the theoretical exponentially rising charging transient.

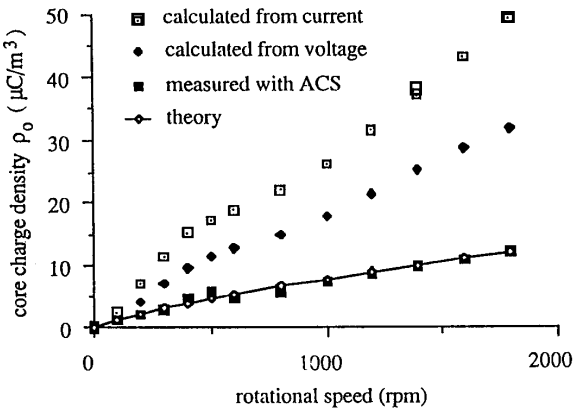

Figure 7.

Core charge density in the small CC measured directly with the ACS and by calculation from measured terminal short-circuit current or open-circuit voltage. Also shown is the solid curve which is the theoretical core charge density as a function of rotational speed. The wall charge density was set to $\rho_w \approx 740\ \mu\text{C/m}^3$ so that (38) (with $\tau_e \approx 30$ s) gave a theoretical ρ_o the same as that measured by the ACS at 1800 rpm [40, 42].

3.2.3 POSSIBLE REASONS FOR DISAGREEMENT BETWEEN TERMINAL MEASUREMENTS AND ANALYSIS

The motivation for the terminal voltage and current measurements was to examine the self-consistency of the analytical model. However, the terminal voltage and current are much more dependent on the details of the geometry and hydrodynamics than is the turbulent core

charge density, as the terminal variables are non-zero only because of the asymmetry of the diffusion sub-layer thicknesses at inner and outer cylinders. If the flow were truly between parallel plate electrodes, the steady state terminal voltage and current would be zero as seen by the right-hand side of (39) and (40) approaching zero as $R_2 \rightarrow R_1$. Thus, even though ρ_o may be finite between parallel plate electrodes, the terminal voltage and current would be zero. The details of the asymmetry in boundary layer thicknesses given by (28) and (29) may not be accurate because of surface roughness or secondary flow end effects in the CC. Such inaccuracies have little effect on the turbulent core charge density but have large effects on the terminal voltage and current. This sensitivity to the asymmetry between diffusive sub-layer thicknesses may be the cause of the disagreement in turbulent core charge densities in Figure 7 between ACS measurements and computations from measured short-circuit currents and open-circuit voltages. This sensitivity may also be the cause of the difference in time constants in Figure 6 for charging and decay of the open-circuit voltage, both values being different from the expected dielectric relaxation time. Our simplified electrokinetic model has also taken ρ_w to be a constant independent of rotational speed and independent of interfacial electric field. It may be that the wall charge density actually depends on field and flow parameters.

3.3 TEMPERATURE TRANSIENT MEASUREMENTS IN THE LARGE CC

3.3.1 EXPERIMENTAL PROCEDURES

Unenergized measurements of the turbulent core charge density ρ_o have been made for a variety of oils and materials covering short-circuited cylinders in the large CC using the computer controlled facility shown in Figure 8. The CC Facility allows easy changes of oil and pressboard covering of inner and outer cylinders. Water cooling through heat exchanging copper tubing wound around the outer cylinder and heating tape also wound around the outer cylinder allow the control of temperatures over the range of 15 to 140°C. Using the various pumps, ports and reservoir the oil and pressboard can be dried with vacuum and heat, and moisture can be added by bubbling moist gas through the system for many hours. Dielectric properties of oil and paper permittivity and conductivity and moisture in oil and paper (MOPS) are measured using microdielectrometry sensors [54] at the inlet and outlet of the CC. Oil charge density in the turbulent core imposed by rotating the inner cylinder is measured with the ACS. The rotation speed of the inner cylinder, temperature, applied voltage magnitude and frequency, and ACS parameters are all under computer control so that a long series of measurements can proceed over many days time without operator attention.

Table 4 is a summary of the data taken in the CC with ACS measured values of ρ_o reported at speeds of 500 or 1000 rpm [39, 41, 42]. The wall charge density ρ_w is found from (38). For the large CC at 1000 rpm, the diffusion sub-layer thickness at the outer cylinder wall is $\delta_2 \approx 7.6\,\mu$m so that the diffusion time is $\tau_d \approx 6800s$. At 500 rpm, $\delta_2 \approx 13\,\mu$m and $\tau_d \approx 11600s$. For both these speeds, $\tau_d \gg \tau_e$ so that (38) yields $\rho_w/\rho_o \approx \tau_d/2\tau_e$. For a typical measured core charge density of $\rho_o \approx 30\,\mu\text{C/m}^3$ at 1000 rpm with a dielectric relaxation time of $\tau_e \approx 10$ s the wall charge density is $\rho_w \approx 0.02$ C/m^3.

The oil dielectric relaxation time was measured at 35°C using the open-circuit voltage decay method described in Section 3.1. Most of the measurements in Table 4 involve a step temperature change up or down from a steady state. The inner cylinder rotation was started $\sim$ 1 h before the temperature was changed. It then took about 30 to 60 min for the system to reach thermal equilibrium at the new temperature. In each of these runs the system was first held at the starting temperature long enough so that steady state conditions were established before the temperature was changed. At equilibrium, there is no net transfer of moisture between the oil and pressboard which results in a constant oil and pressboard moisture content. By increasing the temperature, moisture diffuses out of the pressboard and into the oil until a new equilibrium is established. This increases the oil moisture but only slightly decreases the amount in the pressboard which contains approximately 120× the volume of water than the oil contains. The steady state oil moisture was measured before the temperature was changed and after the oil reached a new steady state at the new temperature, 5 to 60 h later, by taking oil samples to a Mitsubishi moisture meter using the Karl Fischer titration method. Oil moisture levels below 2 ppm are not very accurate because this is the level of precision of the instrument. For many measurements the pressboard moisture was measured at the end of a measurement set by taking a sample of pressboard into an oven accessory attached to the moisture meter. The oil and pressboard moistures were not necessarily in equilibrium when tabulated in Table 4. The charge density during the temperature transient was continually measured using the ACS. Starting and final values are listed in Table 4. Most measurements were taken at constant speeds of the inner cylinder of 1000 rpm but the first early measurements were taken at 500 rpm. The comments column briefly describes oil and paper-drying treatment before measurements began. The normal drying procedure is similar to that used in commercial transformers. The large CC with only pressboard covering the

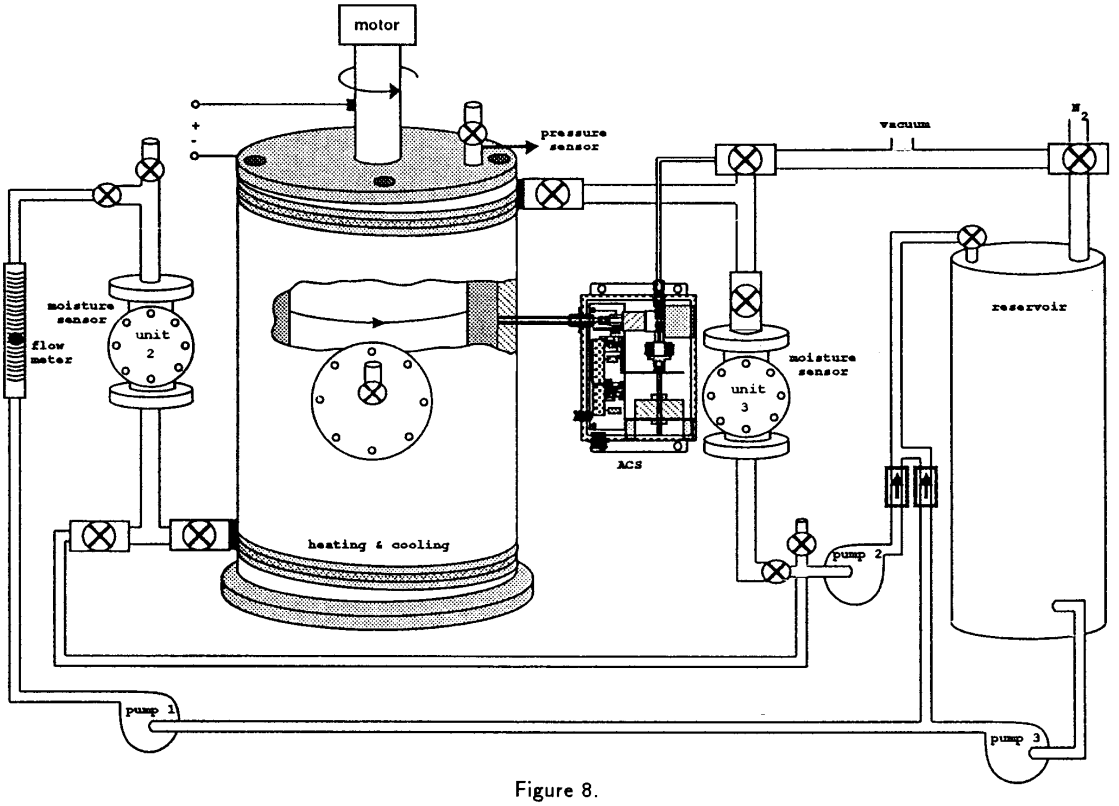

Figure 8.

Couette Charger Facility allowing easy changes of oil and pressboard with cooling and heating capability to control temperatures over the range of 15 to 140°C. Using the various pumps, ports and reservoir the oil and pressboard can be dried with vacuum and heat or moisture can be added by bubbling moist gas through the system. Conductivity, permittivity, and moisture (MOPS) are measured in oil and paper at the inlet and outlet of the CC. Moisture in oil and paper are also measured by taking samples to the moisture meter. Oil charge density is measured with the ACS.

cylinders is heated under vacuum at 90°C to remove naturally absorbed moisture. Then dried oil was added to the CC while still under vacuum to oil-impregnate the pressboard. Some measurements added moisture to the system by bubbling dry nitrogen through water and then bubbling the moist gas through the oil in the CC for many hours. This would increase the moisture in the oil and slowly increase the moisture in the pressboard.

Measurements for Entries 1–10 in Table 4 had an external reservoir under vacuum connected to the CC. This reservoir was used to hold the oil when filling the CC and to dry the oil by pulling a vacuum. A pump continuously circulated the oil in a flow loop from the reservoir under vacuum to the CC and back. The oil entered the CC outer cylinder near the bottom and exited near the top. In order to measure the moisture in the oil, a slight flow was required because the oil sampling port was connected to the flow loop between the outlet of the CC and the reservoir. A low flow rate of 0.062 ml/s was used which had no effect on the measured charge density. This was because the fluid residence time in the CC was $\tau_r \approx 18$ h (volume 5.77 l) which was much longer than the dielectric relaxation time τ_ϵ and diffusion times $\tau_{d1,2}$. As long as $\tau_r \gg \tau_\epsilon$, a slight flow through the CC will not change the charge density generated. With 1 to 6 l of oil in the reservoir, the reservoir residence time was 4.5 to 27 h. For pressboard covered cylinders in entries 1–5 of Table 4, the charge density and short-circuit terminal current had long time constants after a fast change in temperature, like that shown in Figure 9. The long time transients in these entries are believed to be due to this residence time of continuous vacuum drying in the reservoir so that the oil and pressboard in the CC take

Table 4.

Unenergized ACS measurements of the turbulent core charge density in the large CC which shows the starting and ending temperatures with corresponding starting and ending oil and paper moisture. The oil dielectric relaxation time τ_e was measured at 35°C. The wall charge density can be calculated from (38) as $\rho_w/\rho_o = [1 + \tau_d/2\tau_e]$.

		(sec)		(ppm)	(percent)		(μC/m^3)		
1	Oct13a	10	HIVAL Exxon 60	2.5 → 8	0.87	35 → 70	8 → −13	500	oil and paper had been dried
2	Oct14a	9.5	HIVAL Exxon 60	8 → 3	0.87	70 → 40	−6 → 5	500	no further drying from 1
3	Oct26	7.2	HIVAL Exxon 60	46 → 13	1.66	40	5 → 29	500	moist gas had been bubbled through oil from 2
4	Nov7a	7.2	HIVAL Exxon 60	21 → 35	1.66	40 → 70	95 → −31	1000	no further drying from 3
5	Nov14a	7.1	HIVAL Exxon 60	16 → 12.5	1.66	70 → 40	−30 → 19	1000	system failed after 2.5 hours
6	Dec9a	6.7	Bare SS Exxon 60	20	—	70 → 40	10 → 4.9	1000	oil not dried
7	Dec12a	11.8	Bare SS Exxon 60	4	—	35 → 70	1 → 3.4	1000	oil had been dried
8	Dec16a	12.3	Bare SS Exxon 60	1	—	70 → 35	4 — 1.5	1000	no further drying from 7
9	9mar7a	38	Bare SS Shell DA	2.7 → 4.1	—	35 → 70	5.5 → 12.2	1000	oil had been dried
10	9mar24a	3.2	T-IV Shell DA	4.2 → 2.1	0.5	70 → 35	31 → 18	1000	oil and paper had been dried
11	9apr10b	0.56	T-IV Shell DA	2.3 → 2.2	0.5	35 → 15	42 → 25	1000	no further drying from 10
12	9apr12a	0.56	T-IV Shell DA	2.1 → 4.3	0.5	15 → 70	23 → 68	1000	no further drying from 11
13	9apr20b	0.39	T-IV Shell DA	1.7 → 0.9	0.5	70 → 35	34 → (22 − 62)	1000	no further drying from 12,erratic charge densities at 35°C
14	9apr27b	11.2	HIVAL Shell DA	2.9 → 2.3	0.3	70 → 35	4 → −2	1000	oil and paper had been dried
15	9may08b	10	HIVAL Shell DA	2.5 → 1	0.3	35 → 70	−10 → −10	1000	no further drying from 14
16	9jun30b	9.5	HIVAL Shell DA	4.7 → 2	0.54	70 → 35	47 → 34	1000	moist gas had been bubbled through oil from 15
17	9jul13a	8.5	HIVAL Exxon 60	4 → 5	?	35 → 70	17 → −10	1000	oil and paper had been dried
18	9aug14b	5.3	Bare SS Albuquerque	23 → 31	—	35 → 70	8 → 32	1000	used oil not dried
19	9aug18a	5.7	Bare SS Albuquerque	36 → 29	—	70 → 35	22 → 4	1000	no drying from 18

a much longer time to reach moisture equilibrium. For entries 6–9 with bare stainless steel cylinders, the charge

density changed directly with temperature changes. The reservoir was filled with approximately 1 l of oil resulting in a residence time of approximately 4.5 h. In order for all of the oil in the CC and reservoir to reach moisture equilibrium, oil must come in contact with the moisture laden pressboard in the CC. Oil entering the CC was drier than oil leaving, accounting for the long time constant to reach equilibrium. To study the moisture and charge transients in pressboard/oil systems more carefully, the continuous flow of oil through the reservoir under vacuum was stopped for data in Entries 11–19 of Table 4. The charge density and short-circuit terminal current transients with pressboard covered cylinders then directly followed temperature changes. In order to measure the oil moisture, oil was directly sampled from the CC through the port where the continuous flow loop had been connected.

3.3.2 SUMMARY OF EXPERIMENTAL RESULTS

1. Exxon oil was dried and impregnated into dry HIVAL pressboard. The CC ran for 48 h at 500 rpm and 35°C to allow for moisture equilibrium between the oil and pressboard. The temperature was then stepped up from 35 to 70°C increasing the oil moisture from 2.5 ppm to 8 ppm. The paper moisture was 0.87%. With the inner cylinder rotating at 500 rpm the ACS measured the charge density at 35°C to be 8 $\mu C/m^3$. With the step increase in temperature to 70°C the charge density decreased smoothly through zero and reversed polarity reaching $\approx -13\ \mu C/m^3$ after 18 h.

2. With the system of #1 running for 6 more h, the charge density gradually decreased to $-6\ \mu C/m^3$ although the oil moisture remained unchanged at 8 ppm. The temperature was then step decreased to 40°C. The oil moisture content then decreased to 3 ppm. The charge density gradually increased passing through zero after about 10 h and reached a steady state value of 5 $\mu C/m^3$ after about 40 h.

3. After the completion of #2 the oil was taken from the CC and placed into the reservoir. Nitrogen gas first bubbled through water at 50°C was then bubbled through the oil in the reservoir raising the oil moisture level to 46 ppm. The oil was then returned to the CC and measurements began again with the inner cylinder rotating at 500 rpm with the system temperature maintained at 40°C. The oil charge density was initially 5 $\mu C/m^3$ but then rose quickly within 1 h to about 29 $\mu C/m^3$ and remained steady about this value for the experiment run time of about 49 h. The oil moisture measured after 49 h had decreased to 13 ppm while the pressboard moisture level had risen to 1.66%.

4. Experiments began nine days after the completion of #3 with the system temperature maintained at 40°C. The moisture level in the oil was 21 ppm. With the inner cylinder now rotating at 1000 rpm the ACS measured the charge density as 95 $\mu C/m^3$. The temperature was then step increased to 70°C and the charge density decreased through zero after about 2.5 h reaching a steady state of $-31\ \mu C/m^3$ after about 6 h remaining constant thereafter to 19 h. The transient measurement of the charge density and short-circuit terminal current is shown in Figure 9. The data shows that the current and charge density are proportional and opposite in polarity which is consistent with the sign convention in (40) and in Figures 2 and 3.

5. The system was then maintained at 70°C for seven days. The oil moisture decreased to 16 ppm but the charge density was about the same at $-30\ \mu C/m^3$. The temperature was step decreased to 40°C but after 2.5 h, the pressboard came off the outer cylinder and the experiment had to be stopped. At this time the charge density had reversed polarity to $\approx 19\ \mu C/m^3$ and the oil moisture content had decreased to about 12.5 ppm.

6. New Exxon oil from the drum without drying and with bare stainless steel cylinders had a constant moisture level of 20 ppm at 40 and 70°C. This constant moisture level is expected because there was no paper present to absorb or release moisture. The charge density at 70°C was 10 $\mu C/m^3$ and decreased to 4.9 $\mu C/m^3$ at 40°C.

7. The system was then dried for three days decreasing the oil moisture level to 4 ppm and decreasing the charge density at 35°C to 1 $\mu C/m^3$. The temperature was then step increased to 70°C. Within the first hour, the charge density increased to $\approx 4.4\ \mu C/m^3$ in direct proportion to the temperature but then with the temperature essentially constant at 70°C the charge density decreased to about 3.4 $\mu C/m^3$.

8. The system was maintained at 70°C for four days under vacuum which dried the oil to 1 ppm moisture with the charge density at 4 $\mu C/m^3$. The temperature was then step decreased to 35°C and the charge density dropped to $\approx 0.7\ \mu C/m^3$ in synchronism with the temperature drop. With the temperature then essentially constant at 35°C the oil charge density slightly increased to 1.5 $\mu C/m^3$.

9. The oil was then changed to Shell and with bare stainless steel cylinders was dried to 2.7 ppm moisture. At 35°C the oil dielectric relaxation time was 38 s and with

inner cylinder rotation of 1000 rpm the oil charge density was 5.5 $\mu C/m^3$. The temperature was then stepped up to 70°C. The oil moisture level slightly changed to 4.1 ppm and the charge density increased in synchronism with the temperature change to $\approx$ 16 $\mu C/m^3$ then decreasing to a steady state value of 12.2 $\mu C/m^3$.

10. T-IV pressboard was then used with Shell oil and the system was dried with 0.5% moisture in the pressboard and 4.2 ppm moisture in the oil at 70°C. The oil dielectric relaxation time at 35°C dropped to 3.2 s indicating the presence of some ionizable material in the T-IV pressboard. This is contrary to EHV-Weidmann's experience where oil conductivities were found to decrease by a factor of 1.6 when in contact with HIVAL or T–IV pressboard as measured by applying ±750 dc [42,55]. This suggests that some contamination of the system or pressboard had occurred. The charge density at 70°C was 31 $\mu C/m^3$. Note that this positive charge polarity is opposite to that found with Exxon oil and HIVAL pressboard at 70°C. The temperature was then decreased to 35°C. The charge density dropped in synchronism with the temperature decrease to $\approx$ 8 $\mu C/m^3$ gradually increasing to 18 $\mu C/m^3$ after 12 h. The oil moisture decreased to 2.1 ppm. This was the last set of data that had a continuous flow between the CC and reservoir.

11. The experiment then sat for 16 days with no further drying with the dielectric relaxation time dropping further to 0.56 s. The oil moisture remained about constant at 2.3 ppm at 35°C but during the first hour of inner cylinder rotation at 1000 rpm the charge density was erratic with values between 20 and 59 $\mu C/m^3$. The temperature was then step decreased to 15°C and the charge density smoothly decreased in synchronism with the temperature drop to $\approx$ 25 $\mu C/m^3$. The oil moisture level after 18 h was about the same at 2.2 ppm.

12. The system was maintained at 15°C for two days with no further drying. The oil moisture remained about constant at 2.1 ppm. The oil charge density increased during the first hour of inner cylinder rotation at 1000 rpm from 10 to 23 $\mu C/m^3$. With an increase in temperature to 70°C in $\approx$ 30 min, the charge density increased in synchronism with the temperature to $\approx$ 79 $\mu C/m^3$. With the temperature now constant at 70°C the charge density varied for 18 h over the range of 55 to 80 $\mu C/m^3$. The oil moisture increased to 4.3 ppm.

13. The system was maintained at 70°C for the next eight days without further drying. The dielectric relaxation time dropped to 0.39 s. The oil moisture dropped to 1.7 ppm and the charge density dropped to $\approx$ 34 $\mu C/m^3$. The temperature was then decreased to 35°C. The charge density was erratic varying over the range of 20 to 78 $\mu C/m^3$. The oil moisture dropped slightly to 0.9 ppm.

14. The system was changed to new Shell oil and HIVAL pressboard. The system was dried to 2.9 ppm moisture in the oil and 0.3% moisture in the pressboard. The dielectric relaxation time was 11.2 s and the oil charge density was 4 $\mu C/m^3$ at the start of inner cylinder rotation at 1000 rpm rising to $\approx$ 10 $\mu C/m^3$ after 1 h. The charge density decreased to ≈ -2.5 $\mu C/m^3$ in synchronism with the decrease in temperature to 35°C being somewhat erratic to 20 h time over the range of -1 to -5 $\mu C/m^3$ as shown in Figure 10a. The oil moisture level decreased to 2.3 ppm.

15. The system then sat for 8 days at 35°C when the inner cylinder was started rotating at 1000 rpm for 48 h. The oil moisture level was essentially unchanged at 2.5 ppm and the charge density was ≈ -10 $\mu C/m^3$. The dielectric relaxation time was also essentially unchanged at 10 s. With the inner cylinder rotating at 1000 rpm the temperature was then increased to 70°C. The charge density magnitude then decreased in synchronism with the temperature to ≈ -2.5 $\mu C/m^3$ as shown in Figure 10b. Then with the temperature constant at 70°C the charge density smoothly decreased back to ≈ -10 $\mu C/m^3$ after 18 h. The oil was very dry and unlike all other temperature rise experiments, the moisture content at 1 ppm was less at the higher temperature which may account for the strange charge density transient.

16. Moist gas was then bubbled through the oil to raise the oil moisture level to 4.7 ppm at 70°C and the pressboard moisture to 0.54%. The charge density increased to 40 $\mu C/m^3$ at the start of inner cylinder rotation at 1000 rpm. The charge density slightly increased to 47 $\mu C/m^3$ after 1 h of rotation when the temperature was decreased to 35°C as shown in Figure 10c. The charge density then decreased to $\approx$ 34 $\mu C/m^3$. Also shown in Figure 10c is the time dependence of the oil moisture level with the step decrease in temperature. The oil moisture tracked the oil temperature as did the charge density and short-circuit terminal current. Since a diffusion process governs the relations between oil and pressboard moisture, the oil moisture can not change instantaneously. The time for the oil moisture to reach a steady state value after this step change in temperature was calculated [56] to be $\approx$ 1.3 h. In this experiment, the temperature step change took $\sim$ 1 to 2 h which was not fast enough to see the transient governed by the diffusion of moisture in the oil and pressboard.

17. The system was changed to new Exxon oil and HIVAL pressboard with dielectric relaxation time at 35°C

of 8.5 s. The system was dried for 10 h rather than the usual 16 h to allow the oil moisture level to be 4 ppm at 35°C. The pressboard moisture level could not be measured because of malfunction of the moisture meter. The charge density was erratic for the first hour of inner cylinder rotation at 1000 rpm varying from 1 to 18 $\mu C/m^3$. The temperature was then step increased to 70°C and the charge density slowly decreased to zero after $\approx$ 5 h reaching a steady value of $-10\,\mu C/m^3$ after $\sim$ 24 h. The oil moisture only slightly increased to 5 ppm. This measurement had test conditions similar to that of measurements #4–5 with similar results. Confidence was gained by this reproducibility for measurements taken eight months later.

18. The system was then changed to used oil from an Albuquerque transformer using bare stainless steel cylinders without drying with dielectric relaxation time of 5.3 s. The initial oil moisture at 35°C was 23 ppm and the charge density at 1000 rpm inner cylinder rotation rate was steady at $\approx$ 8 $\mu C/m^3$. The temperature was then step increased to 70°C and the charge density varied over the range of 32 to 37 $\mu C/m^3$ as the oil moisture level increased to 31 ppm.

19. After sitting for four days at 70°C the oil moisture was 36 ppm and the charge density varied over the range of 16 to 21 $\mu C/m^3$ during the first hour of inner cylinder rotation at 1000 rpm. The temperature was then step decreased to 35°C reducing the charge density to about 4 $\mu C/m^3$ as the moisture dropped slightly to 29 ppm.

3.3.3 RELATIONSHIP OF CORE CHARGE DENSITY TO SHORT-CIRCUIT TERMINAL CURRENT

The measurements in Figures 9 and 10 also show the short-circuit terminal current magnitudes in the large CC at 1000 rpm to be $\sim$ 3000 pA. Figure 5 shows the same measurement in the small CC to be ~ -28 pA at 1000 rpm. Equation (40) gives the predicted relationship between steady state short-circuit terminal current i, turbulent core charge density ρ_o, dielectric relaxation time τ_e, and geometric dimensions of the CC. Separating out measured variables from the geometric factor G, (40) can be written in the form

$$\frac{-i\tau_e}{\rho_o} = G = \frac{\pi l\left[(R_2^2 + R_1^2)\ln(R_2/R_1) - (R_2^2 - R_1^2)\right]}{2\ln(R_2/R_1)} \tag{42}$$

For all CC dimensions in centimeters, the geometric factor G is 275 for the large CC and 61.5 for the small CC. The measured charge density in Figure 7 at 1000 rpm is $\approx$ 8 $\mu C/m^3$. With a measured dielectric relaxation time of 30 s and a measured terminal current of -28 pA, $(-i\tau_e/\rho_o) = 105$. This is of the same order of the predicted value of 61.5. The deviation can be attributed to the measurement sensitivity discussed in Section 3.2.3.

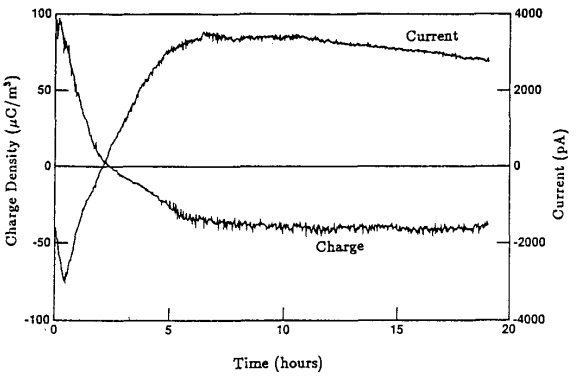

Figure 9.

Entry 4 of Table 4. Charge density and short-circuit terminal current responses to a step change in temperature from 40 to 70°C. Oil moisture started at a non-equilibrium value of 21 ppm and ended at a value of 35 ppm which was approaching equilibrium. Exxon Univolt 60 and HIVAL pressboard at 1.66% moisture were used with a rotational speed of 1000 rpm. With this oil/pressboard combination and at 70°C, charging becomes negative as the oil moisture approaches equilibrium.

Table 5 lists the measured steady state values of $(-i\tau_e/\rho_o)$ at two temperatures in the large CC which should be compared to the predicted value of G=275. Accounting for the measurement sensitivity discussed in Section 3.2.3, the measurements in Table 5 are in reasonable agreement with analysis.

3.3.4 OBSERVATIONS OF ELECTRIFICATION DEPENDENCE ON TEMPERATURE, MOISTURE, AND DIELECTRIC RELAXATION TIME

1. A reversal in the polarity of the charge density was only observed when HIVAL pressboard was tested. T-IV covered and bare stainless steel cylinders always gave positive charge densities in the oil, that increased with temperature.

Table 5.
Measurement of turbulent core charge density and short-circuit terminal current in the large CC. The predicted value in the large CC is $(-i\tau_e/\rho_o)$ =G=275. The value of τ_e at 70°C was taken from Table 6 or if not measured at 70°C was estimated as 1/5 the measured value at 35°C as given in Table 4.

#	T °C	ρ_o μC/m^3	i pA	τ_e s	$-i\tau_e/\rho_o$
2	70	−5	120	2	48
	35	5	−75	9.5	142
4	40	95	−3200	7.2	243
	70	−31	3400	1.5	165
16	70	48	−10, 750	1.4	307
	35	34	−1, 000	9.5	279
18	35	8	−400	5.3	265
	70	27	−4, 400	1.2	196
19	70	16	−2, 800	1.3	228
	35	4	−500	5.7	713

2. From measurements with bare stainless steel cylinders so that the oil moisture level remained essentially constant even with changes in temperature (#6–8, 9, 18–19), the oil charge density was positive and increased with increasing temperature. At a given temperature, the oil charge density was higher when the oil moisture level was higher (compare #6, 18, and 19 to #7 and 8).

3. The oil charge densities were much higher and the oil dielectric relaxation times were much smaller with T-IV pressboard than with HIVAL pressboard and bare metal cylinders. This indicates the presence of ionizable impurities from the T-IV pressboard that increases the oil conductivity and increases the wall charge density, perhaps by enhanced adsorption into the T-IV pressboard.

4. The oil charge density increased as the moisture level in the pressboard increased (see #3).

5. When the oil system was contained during the measurements (#11–19), the charge density transient was generally in synchronism with the temperature transient except for #17 which was only dried for 10 h rather than the usual 16 h where it took about 8 h for the charge density to reach an essentially steady value.

6. The typical slight increase of the charge density and oil moisture during the first hour of the experiment is shown in Figure 10a,c in which the rotation of the inner cylinder was started at time zero. During this period, the oil temperature was held at 70°C by cooling the outer cylinder of the large CC. The CC must be cooled while the inner cylinder is rotating to remove the heat generated by the fluid shear stresses on the inner and outer cylinders. Since the inner cylinder was not directly cooled, the pressboard surface temperature on the inner cylinder was greater than the oil in the core as recorded by the temperature sensor in Figure 10. This would probably result in increased oil moisture due to diffusion of moisture out of the inner cylinder pressboard and into the oil. The core charge density could also be affected by this increased surface temperature.

4. ENERGIZATION CHARGING

We might picture the oil-impregnated pressboard to not only have a layer of net charge on the fluid side of the interface, but to also have interstices filled with ions. For net positive charge accumulation due to HV energization, positive ions are presumably more readily coerced into the adjacent oil by an electric field so that more positive than negative charge is injected during a cycle. In the case of bare metal electrodes, the charges may be due to ionization of materials adsorbed on the oxide surface. Tentatively, the parameter being measured is the 'injection charge density' ρ_{inj}, to be estimated from measurements as the field amplitude and frequency are varied [39, 41, 42].

4.1 CHARGE INJECTION MODEL

As a limiting case, consider the boundary in Figure 11 which only injects positive charge with mobility b when the electric field points away from the boundary. When the sinusoidally varying electric field $E_o \cos \omega t$ perpendicular to the wall is positive, positive charge is injected and migrates away from the wall. When the electric field reverses polarity, the charge returns to the wall. Charges are injected from $x = 0$ at different times t_o in the voltage cycle and thus penetrate different distances into the flow. In addition, the already present equilibrium double-layer charge not included in earlier analysis [34–36] will migrate in the imposed electric field somewhat analogously to an ac field modulated double layer model developed for laminar flow [57]. Some of this additional charge will be injected into the turbulent core for any applied voltage as seen in earlier measurements [34–36]. This resolves the disagreement with past analysis that predicted a threshold field strength before energization charging would occur as only charge injected from the boundary was considered, neglecting charge injected from the 'equilibrium' double layer.

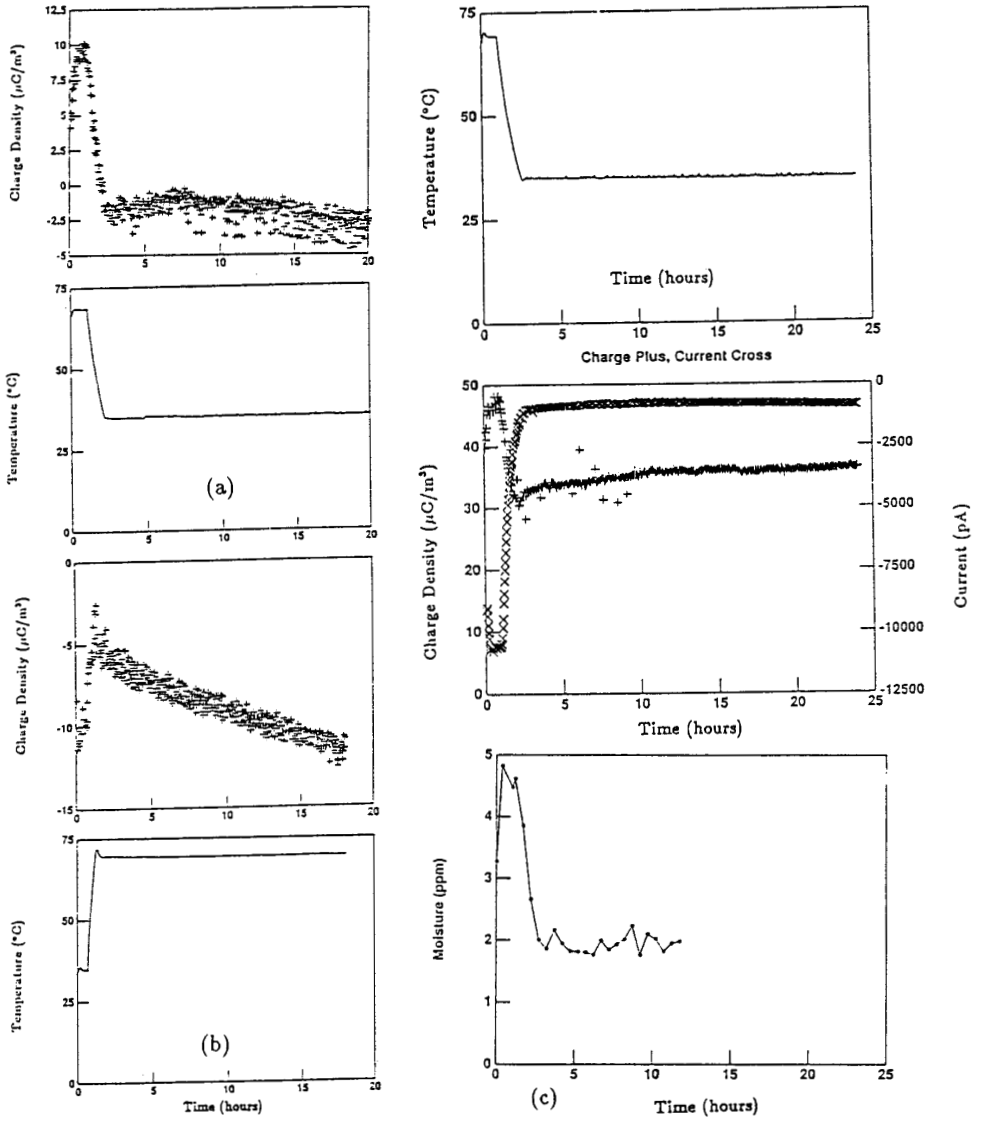

Figure 10.

Large CC with HIVAL pressboard covered cylinders and Shell Diala A oil with 1000 rpm rotational speed comparing dried oil with a (a) step decrease and (b) step increase in temperature and (c) moist oil after moist gas had been bubbled through to raise oil moisture from 1 to 4.7 ppm at 70°C and to raise pressboard moisture from 0.3 to 0.54%. (a) Entry 14 of Table 4 with 70 to 35°C step decrease in temperature. The oil moisture decreased from 2.9 to 2.3 ppm. The paper moisture was 0.3% and the dielectric relaxation time was 11.2 s. (b) Entry 15 of Table 4 with a 35 to 70°C temperature step increase. The oil moisture decreased from 2.5 to 1 ppm and the dielectric relaxation time was 10 s (at 35°C); (c) Entry 16 of Table 4 with paper moisture raised to 0.54%. Oil temperature step decrease from 70 to 35°C, core charge density and terminal current as a function of time, oil moisture transient which decreased from 4.7 to 2 ppm. The oil dielectric relaxation time was 9.5 s (at 35°C).

Neglecting self-field effects from the space charge and the small amount of turbulent diffusion near the wall, the

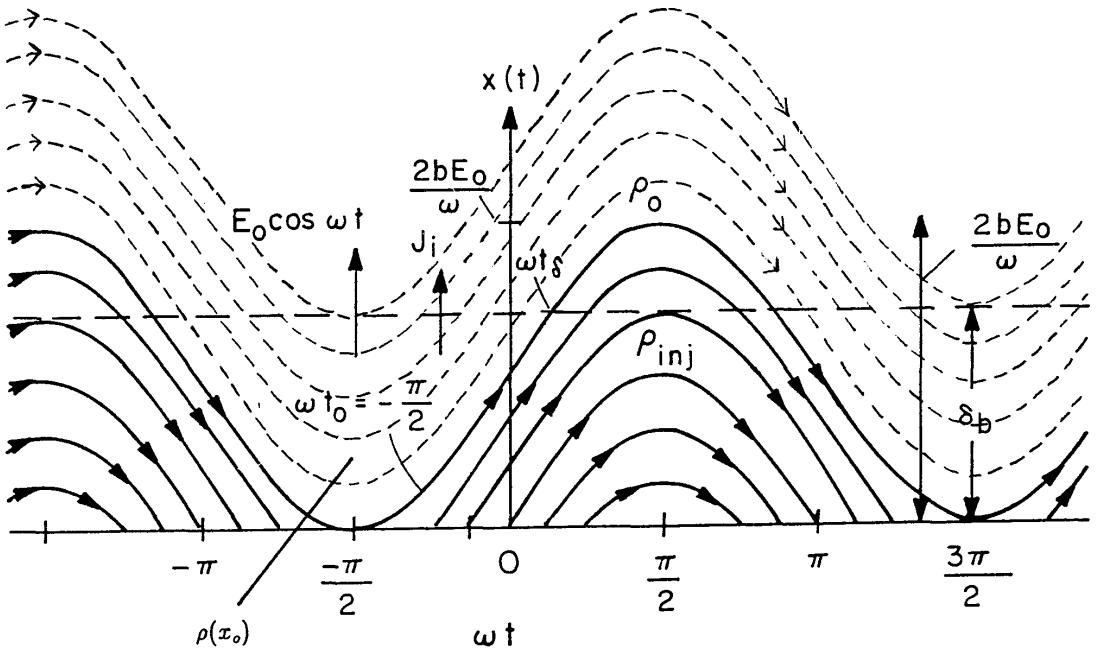

Figure 11.

ac charge injection trajectories starting at the oil/pressboard interface $x = 0$ at time t_o with density ρ_{inj} and injection trajectories starting within the migration based sublayer of thickness δ_b at x_o at time $t = -\pi/2\omega$ with charge density $\rho(x_o)$.

charge velocity

$$\frac{dx}{dt} = bE = bE_o \cos \omega t \tag{43}$$

yields by integration the charge trajectories

$$x(t) = \int_{t_o}^{t} bE_o \cos \omega t \, dt = \frac{bE_o}{\omega}(\sin \omega t - \sin \omega t_o) + x_o \tag{44}$$

where t_o is the time the charge is injected from the $x_o = 0$ boundary and $x_o \neq 0$ is the initial position of the equilibrium charge in the double layer at time $t_o = -\pi/2\omega$. Because the peak distance that the charge migrates, $\delta_{mig} = 2bE_o/\omega$, is much less than the inner radius of the cylinders or the gap d, even for large fields at low frequency, the boundaries are treated as flat and non-interacting. Because the dielectric relaxation time $\tau_e = \varepsilon/\sigma$, and self-precipitation time $\tau_p = \varepsilon/\rho b$, are generally much longer than the charge flight times we take the charge density along a trajectory to be constant.

If charge reaches beyond a boundary layer thickness δ_b into the turbulent core, it becomes entrained in the flow and does not return to the wall. This thickness is defined in (25) as that distance at which the peak migration velocity bE_o just equals the fluid fluctuation rms velocity component perpendicular to the wall $(\overline{v_x'^2})^{1/2}$ as given in (9). The boundary layer thickness for the Taylor correlation of (14) is then

$$\delta_b = 63dR^{-9/8}(bE_o d/\nu)^{1/2} \tag{45}$$

where $R = \Omega R_2 d/\nu$ is the Reynolds number. Representative values for our experiments have an ion mobility of $b \approx 10^{-9}\,\mathrm{m^2/(Vs)}$, maximum electric field $E_o = 0.5 \times 10^6\,\mathrm{V/m}$, and maximum inner cylinder speed of 1800 rpm, which gives $\delta_b \approx 30\,\mu\mathrm{m}$.

If the field E_o is too low or the frequency ω is too high so that the maximum charge migration length is less than the sublayer thickness ($2bE_o/\omega < \delta_b$), charge trajectories given by (44) for charge injected at the $x = 0$ wall do not cross the boundary layer into the turbulent core and thus do not contribute to injected current. However, the equilibrium charge density taken to linearly vary from the wall charge density ρ_w at $x = 0$ to the turbulent core charge density ρ_o at $x = \delta_b$ as

$$\rho = \rho_w + (\rho_o - \rho_w)x_o/\delta_b \quad 0 \leq x_o \leq \delta_b \tag{46}$$

has some charge that crosses $x = \delta_b$. Since we take the charge density to remain constant along a trajectory we can use (44) to relate position x at time t to initial position x_o at time $\omega t_o = -\pi/2$ so that the charge density of (46) at later positions and time is

$$\rho = \rho_w + \frac{\rho_o - \rho_w}{\delta_b}\left[x - \frac{bE_o}{\omega}(\sin\omega t + 1)\right] \qquad (47)$$

In particular, with $x = \delta_b$, the current density $J_i = \rho b E_o \cos\omega t$ crosses into the turbulent core over the time interval $-\pi/2 \le \omega t \le \pi/2$. For the time interval $\pi/2 \le \omega t \le 3\pi/2$, charge with density ρ_o in the turbulent core crosses back over into the sublayer. We assume that once in the sublayer, equilibrium diffusion processes convert this charge density of ρ_o back to the linear profile of (46) before the field reverses direction. Then the net current that crosses the sublayer into the turbulent core is

$$\begin{aligned} J_i = \frac{\omega}{2\pi}\Bigg[&\int_{-\pi/2\omega}^{\pi/2\omega}\{\rho_w(\rho_o - \rho_w)[1 - \frac{bE_o}{\omega\delta_b}(\sin\omega t + 1)]\} \\ &bE_o\cos(\omega t)\,dt \\ &+ \int_{\pi/2\omega}^{3\pi/2\omega}\rho_o bE_o\cos\omega t\,dt\Bigg] \\ = &\frac{(\rho_w - \rho_o)b^2E_o^2}{\pi\omega\delta_b} \end{aligned} \qquad (48)$$

If the field E_o is high enough, or frequency ω is low enough, such that $2bE_o/\omega > \delta_b$ then injected charge with density ρ_{inj} can also cross the sublayer which results in additional current charging the turbulent core. Equilibrium charge now crosses $x = \delta_b$ into the turbulent core in the time interval $-\pi/2 \le \omega t \le \omega t_\delta$ and injected charges cross $x = \delta_b$ into the turbulent core in the time interval $\omega t_\delta \le \omega t \le \pi/2$. Turbulent core charge crosses $x = \delta_b$ back into the sublayer in the time interval $\pi/2 \le \omega t \le 3\pi/2$. The time t_δ is found for that trajectory starting at $x_o = 0$, $\omega t_o = -\pi/2$ to reach $x = \delta_b$

$$\delta_b = \frac{bE_o}{\omega}(\sin\omega t_\delta + 1) \;\Rightarrow\; \sin\omega t_\delta = \frac{\omega\delta_b}{bE_o} - 1 \qquad (49)$$

The net current density crossing $x = \delta_b$ is then

$$\begin{aligned} J_i = \frac{\omega}{2\pi}\Bigg[&\int_{-\pi/2\omega}^{t_\delta}\{\rho_w + (\rho_o - \rho_w)[1 - \frac{bE_o}{\omega\delta_b}(\sin\omega t + 1)]\} \\ &bE_o\cos\omega t\,dt \\ &+ \int_{t_\delta}^{\pi/2\omega}\rho_{inj}bE_o\cos\omega t\,dt + \int_{\pi/2\omega}^{3\pi/2\omega}\rho_o bE_o\cos\omega t\,dt\Bigg] \\ = &\frac{bE_o}{2\pi}\left[\frac{\omega\delta_b}{bE_o}\left(\frac{\rho_o + \rho_w}{2} - \rho_{inj}\right) + 2(\rho_{inj} - \rho_o)\right] \end{aligned} \qquad (50)$$

Charge conservation requires that the time rate of change of the charge in the volume V be equal to the sum of the injected, diffusion, and ohmic currents

$$V\frac{d\rho_o}{dt} = 2\pi l(J_1R_1 + J_2R_2) - V\rho_o\sigma/\varepsilon \qquad (51)$$

where $J_{1,2} = J_{i1,2} + J_{d1,2}$ is the sum of the injected and diffusion current densities evaluated at the inner and outer cylinders. Provided that the space charge field is negligible compared to the imposed field, the electric field at the inner and outer cylinders with an applied voltage V is

$$E_{1,2} = \frac{V}{R_{1,2}\ln(R_2/R_1)} \qquad (52)$$

Reducing (51), the governing equation for the core charge density is related to the wall charge densities $\rho_{w1,2}$, injection charge densities $\rho_{inj1,2}$, diffusion times $\tau_{d1,2}$, dielectric relaxation time τ_e, and injection times $\tau_{a1,2}$, $\tau_{b1,2}$, and $\tau_{c1,2}$ by

$$\begin{aligned} &\frac{d\rho_o}{dt} + \left(\frac{1}{\tau_e} + \frac{1}{\tau_{d1}} + \frac{1}{\tau_{d2}} + \frac{1}{\tau_{a1}} + \frac{1}{\tau_{a2}}\right)\rho_o = \frac{\rho_{inj1}}{\tau_{c1}} \\ &+\frac{\rho_{inj2}}{\tau_{c2}} + \rho_{w1}\left(\frac{1}{\tau_{d1}} + \frac{1}{\tau_{b1}}\right) + \rho_{w2}\left(\frac{1}{\tau_{d2}} + \frac{1}{\tau_{b2}}\right) \\ &\tau_{d1,2} = \frac{\delta_{1,2}(R_2^2 - R_1^2)}{2DR_{1,2}} \\ &\tau_e = \frac{\varepsilon}{\sigma} \end{aligned} \qquad (53)$$

$$\tau_{a1,2} = \begin{cases} \frac{\pi\omega\delta_{b1,2}(R_2^2 - R_1^2)}{2b^2E_{1,2}^2R_{1,2}} & \delta_{b1,2} > \frac{2bE_{1,2}}{\omega} \\ \frac{\pi(R_2^2 - R_1^2)}{(4bE_{1,2} - \omega\delta_{b1,2})R_{1,2}} & \delta_{b1,2} < \frac{2bE_{1,2}}{\omega} \end{cases} \qquad (54)$$

$$\tau_{b1,2} = \begin{cases} \frac{\pi\omega\delta_{b1,2}(R_2^2 - R_1^2)}{2b^2E_{1,2}^2R_{1,2}} & \delta_{b1,2} > \frac{2bE_{1,2}}{\omega} \\ \frac{2\pi(R_2^2 - R_1^2)}{\omega\delta_{b1,2}R_{1,2}} & \delta_{b1,2} < \frac{2bE_{1,2}}{\omega} \end{cases} \qquad (55)$$

$$\tau_{c1,2} = \begin{cases} \infty & \delta_{b1,2} > \frac{2bE_{1,2}}{\omega} \\ \frac{\pi(R_2^2 - R_1^2)}{(2bE_{1,2} - \omega\delta_{b1,2})R_{1,2}} & \delta_{b1,2} < \frac{2bE_{1,2}}{\omega} \end{cases} \qquad (56)$$

4.2 MEASUREMENTS FITTED TO ANALYSIS

Measurements were made in the CC for a variety of oil types with pressboard covered or bare metal cylinders. An applied ac voltage between the cylinders was used to study the effect of energization. The frequency is stepped from 0.5, 1.0, 2.0, to 4.0 Hz. For each frequency, the voltage is stepped from 0 to 4 kV peak in 1 kV steps, while for each voltage and frequency, the rotational speed is stepped from 0 to 1500 rpm in 100 rpm steps. This matrix of measurements takes 38 h to complete and is under computer control.

This model has been fitted to data of measured charge density *vs.* cylinder speed for zero applied voltage as well as applied voltages of 1 to 4 kV peak for frequencies over the range of 0.5 to 4 Hz as shown in Figure 12 by using a three-parameter estimation of the wall charge density ρ_w, injection charge density ρ_{inj}, and diffusion coefficient D. These values were calculated to minimize the magnitude difference error between analysis and measurements. Since both inner and outer cylinders were bare stainless steel or covered with the same pressboard, wall and injected charge densities were taken to be equal at each cylinder $\rho_w = \rho_{w1,2}$ and $\rho_{inj} = \rho_{inj1,2}$.

In order to achieve a good fit between experiment and theory, it was also necessary to estimate the diffusion coefficient within the diffusion sublayer. If the walls were perfectly smooth and the sub-layer truly laminar, one would expect the diffusion coefficient to have a value of the molecular diffusivity, $D_m = 2.5 \times 10^{-11}\text{m}^2/\text{s}$ for our oil, but estimations, listed in Table 6, show that it is from 4 to 33× greater for bare metal cylinders, and from 3 to 113× greater for pressboard covered cylinders. A larger diffusion coefficient is expected due to the turbulent mixing in the core which penetrates into the sublayer. In addition, we expect the rough surface of the pressboard to enhance the diffusion of charge at the oil/pressboard interface because the roughness scale is on the same order as the sublayer thickness. This conclusion is supported by measurements in Table 6 for T–IV pressboard, which has a surface roughness larger than the HIVAL pressboard and also has the largest values of fitted diffusion coefficient.

4.2.1 LOW ROTATIONAL SPEED MEASUREMENTS

The model of (53) in the steady state was only fitted to data points which had a rotational speed of 500 rpm or greater. Below 500 rpm, the data was widely varying due to cellular convection. The measured charge densities in this rotational speed range were often very large and not reproducible. This behavior is shown in Figure 12 for $\Omega < 500$ rpm. Charge densities at 0.5 Hz. and 100 rpm were larger than at higher rotational speeds. From Section 3.3.1, the transition from cellular convection to turbulent flow in the large CC occurs at 62 rpm. Below this speed, the flow has laminar vortices (Taylor cells) and is not fully mixed which may result in an inhomogeneous charge distribution across the gap between the cylinders. As the rotational speed is increased above 62 rpm, the Taylor cells begin to break up and a turbulent flow is developed. It is believed that a highly mixed, fully developed turbulent flow does not occur until the rotational speed is 500 rpm or greater which is the threshold where the measured data had little 'noise'.

4.2.2 RESULTS

Table 6 is a summary of data taken in the CC units for a variety of oils and materials covering the cylinders with the results of the three parameter estimation listed. The dielectric relaxation times shown in this table were measured at the operating temperature and were used for calculations in the parameter estimation. The kinematic viscosity ν of the oil was taken to have a temperature dependence [28] of $\nu = \nu_o \exp(W/kT)$ where $\nu_o = 3.956 \times 10^{-10}$ m^2/s, $W = 0.2725$ eV, T is the oil temperature (K), and $k = 8.617 \times 10^{-5}$ eV/K is Boltzmann's constant. At 22°C this gives a kinematic viscosity of 1.80×10^{-5} m^2/s. At 35 and 70°C, the kinematic viscosities are 1.14×10^{-5} m^2/s and 3.99×10^{-6} m^2/s respectively.

All of the runs that used bare stainless steel cylinders gave positive charge densities that increased with increasing HV applied between the cylinders as shown by Entries 2, 4, 10, and 11. The data for Entry 2 is shown in Figure 12. The measured charge density increased with increasing rotational speed, increasing applied voltage amplitude, and decreasing applied voltage frequency. The estimated valves of ρ_w and ρ_{inj} were both positive. As shown by Entries 10 and 11, the values of both ρ_w and ρ_{inj} were greater at 70 than at 35°C.

HIVAL covered cylinders and Shell Diala A oil gave negative charge densities that increased negatively with applied voltage for both 35 and 70°C as shown by Entries 7 and 8. The data for Entry 8 is shown in Figure 13. The estimated values of ρ_w and ρ_{inj} were both negative at 35°C and became more negative at 70°C.

T–IV pressboard and Shell oil gave positive charge densities that increased with applied voltage at 35°C as shown

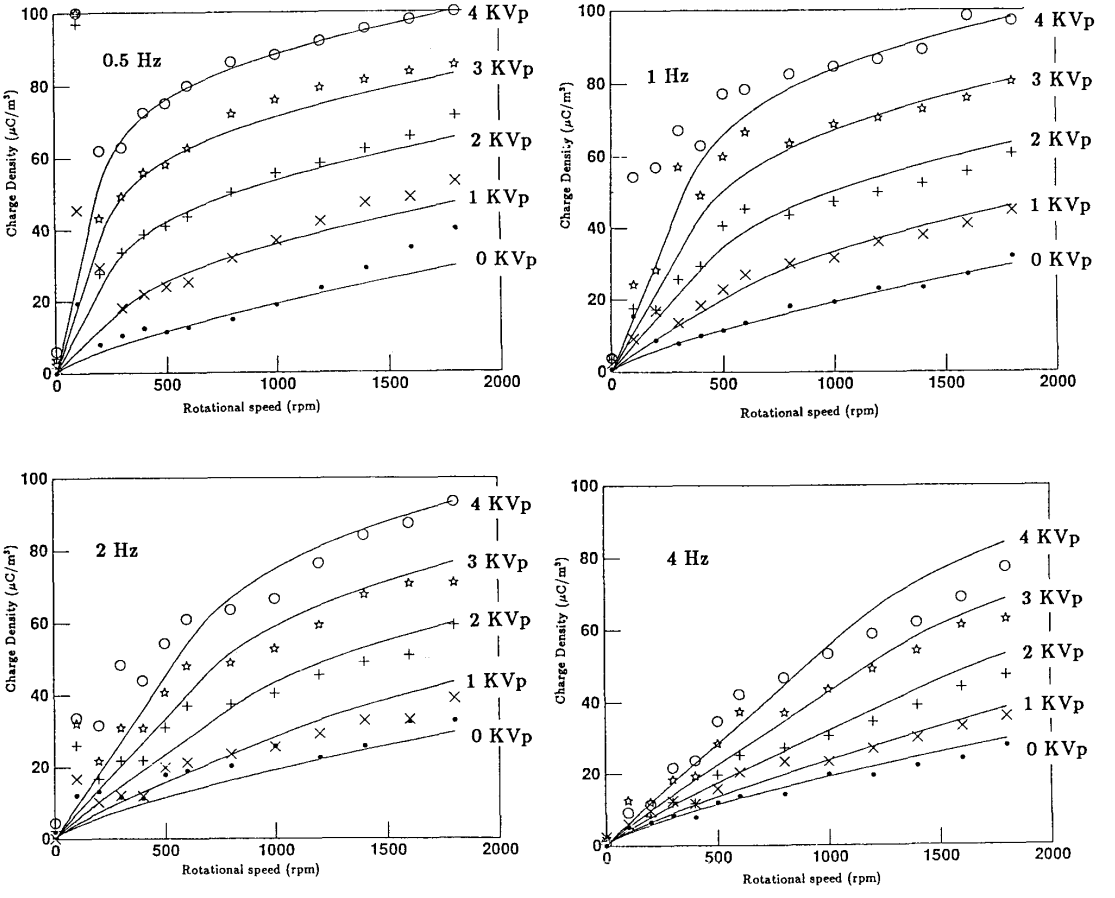

Figure 12.

Entry 2 of Table 6. Positive core charge density measured in the CC with bare stainless steel cylinders and Exxon Univolt 60 transformer oil at 6 ppm moisture with a dielectric relaxation time of 12 s. Data was taken at 30°C with $v = 0$ (dots) and with an applied ac voltage of 1 (crosses), 2 (pluses), 3 (stars), and 4 (circles) kV peak at 0.5, 1, 2, and 4 Hz with the rotational speed varied from 0 to 1800 rpm. The solid lines are calculated from (53) in the steady state using a three parameter best fit of $\rho_w = 1.92\,\mathrm{mC/m^3}$, $\rho_{inj} = 1.68\,\mathrm{mC/m^3}$, and $D = 1.23 \times 10^{-10}\,\mathrm{m^2/s} = 4.9\mathrm{D_m}$.

by Entry 5. At 70°C, the positive charge density decreased with applied voltage as shown by Entry 6 and Figure 14, including polarity reversal. For this pressboard, oil, and temperature combination, the wall charge density $\rho_w = 20\ \mathrm{mC/m^3}$ was positive whereas the injection charge density $\rho_{inj} = -46\ \mathrm{mC/m^3}$ was negative.

T–IV pressboard and Exxon oil, as shown by Entry 3, gave less charge than T–IV pressboard and Shell oil as shown by Entry 5. HIVAL pressboard covered cylinders and Exxon Univolt 60 oil at 35°C gave positive charge that increased slightly with increasing applied voltage as shown by Entry 9. This combination was not tested at 70°C. Positive values of ρ_w for T–IV covered and bare stainless steel cylinders and negative values for HIVAL covered cylinders are consistent with the unenergized measurements of Section 3.3.

5. CONCLUDING REMARKS

A Couette Charger facility was built to simulate flow electrification processes in transformers, where transformer oil filled the annulus between coaxial cylindrical electrodes that were covered with bare metal or transformer pressboard. The inner cylinder rotates at speeds

Table 6.

Estimated parameters for energized measurements in the CC for a variety of oils and materials covering the cylinders. Entry 1 is data taken in the small CC with 50 ppm BTA. All other entries are in the large CC without additives. The core charge density, ρ_o, with a rotation speed of 1500 rpm, is also shown for zero voltage (unenergized) and for an ac voltage of 4 kV peak at 0.5 Hz applied between the cylinders (energized).

#	Name	Materials	Oil Moisture (ppm)	Temp. (°C)	τ_e (sec)	ρ_w (mC/m^3)	ρ_{inj} (mC/m^3)	D/10^{-12} (m^2/s)	D/D$_m$ (D$_m$ = 25× 10^{-12} m^2/s)	ρ_o (μC/m^3) unenergized	ρ_o (μC/m^3) energized
1	bmar22	Manning 220 Gulf TH with 50 ppm BTA	50	30	39	0.105	0.255	741	29.6	16	92
2	bjun22	Bare SS Exxon 60	6	30	12	1.92	1.68	123	4.9	32	97
3	sept2b	T-IV Exxon 60	6	30	4	2.6	2.57	1200	48.0	58	95
4	jan4a	Bare SS Shell DA	11	30	56	0.040	0.191	816	32.6	8	37
5	9apr08a	T-IV Shell DA	2.3	35	1.16	7.09	5.24	2447	97.9	97	92
6	9apr13b	T-IV Shell DA	2.7	70	.22	20	-46	2828	113.1	77	13
7	9may05a	HIVAL Shell DA	2.5	35	10	-1.26	-1.50	280	10.9	-15	-23
8	9may12b	HIVAL Shell DA	1	70	1.44	-6.75	-4.56	75	3.0	-17	-35
9	9jul10c	HIVAL Exxon 60	6.8	35	8.5	0.454	0.139	1293	51.7	46	29
10	9aug10a	Bare SS Albuquerque	23	35	4.08	0.752	2.14	520	20.8	10	58
11	9aug15b	Bare SS Albuquerque	36	70	1.2	16.4	17.4	93	3.7	25	89

giving controlled turbulent flow which brings electric charge to the volume from the electrical double layer at the liquid/solid interfaces.

Flow electrification charge density measurements as a function of inner cylinder speed were made using the absolute charge sensor which brings a sample of fluid from the turbulent core into a Faraday cage and measures the total charge with no extraneous contributions from charge separated within the ACS itself.

Transient measurements with a step change in temperature have shown the charge density to change from an initial value to a new steady state value, both values probably dependent on the equilibrium moisture levels in oil and pressboard. For all bare metal and T-IV pressboard cases, the oil charge density was positive but with HIVAL pressboard there were some moisture and temperature regimes where the charge polarity reversed.

The effects of transformer energization were also simulated by applying low frequency (0.5 to 4 Hz) HV (field strength $\leqslant$ 1.8 kV/cm peak) across the cylinders of the CC. Generally this energization increased the magnitude of net charge in the turbulent core which increased with decreasing frequency, but the T-IV pressboard and Shell oil combination had a decrease in charge density with increasing voltage including polarity reversal. This indicates that injected charge can be the same or opposite polarity to the charge on the liquid side of the equilibrium double layer. To help understand the effects of energization and to scale laboratory measurements at low voltages and low frequencies to operating transformers, a charge injection model was developed that examined the migration of double layer and injected charge in the imposed

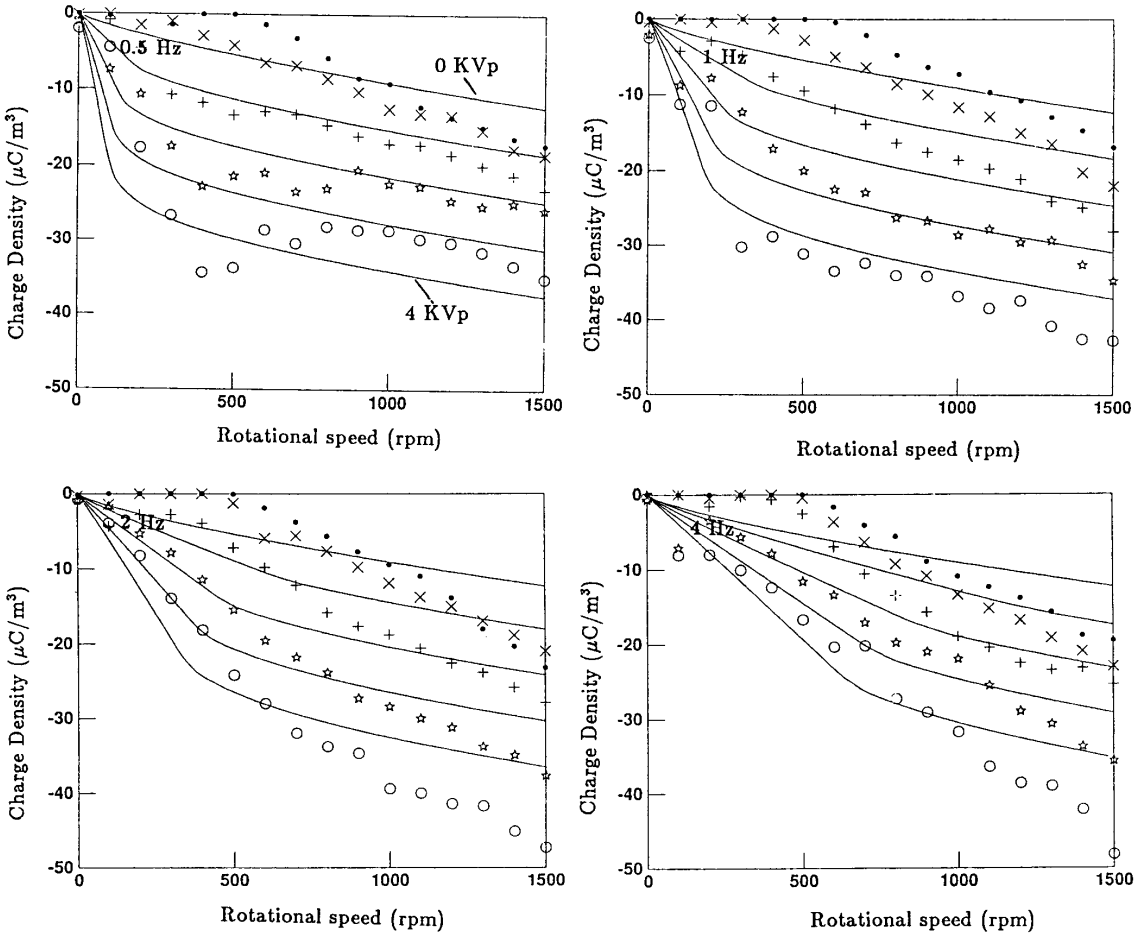

Figure 13.

Entry 8 of Table 6. Negative core charge density measured in the large CC with HIVAL covered cylinders and Shell Diala A transformer oil at 1 ppm moisture with a dielectric relaxation time of 1.44 s. Data was taken at 70°C with $v = 0$ (dots) and with an applied ac voltage of 1 (crosses), 2 (pluses), 3 (stars), and 4 (circles) kV peak at 0.5, 1, 2, and 4 Hz with the rotational speed varied from 0 to 1500 rpm. The solid lines are calculated from (53) in the steady state using a three parameter best fit of $\rho_w = -6.7\,\mathrm{mC/m^3}$, $\rho_{inj} = -4.6\,\mathrm{mC/m^3}$, and $D = 7.5 \times 10^{-11}\,\mathrm{m^2/s} = 3.0\mathrm{D_m}$.

sinusoidally time-varying electric field.

Good fits between this model and measurements were achieved by finding best fits of equilibrium charge density at the solid/liquid interface, injected charge density due to energization, and diffusivity in the diffusive sublayer near the wall. The diffusivity exceeded the molecular diffusivity by ~ 5 to $30\times$ for bare metal cylinders, and by $\lesssim 113$ for pressboard covered cylinders. This enhanced diffusivity was probably due to the turbulent mixing of the core penetrating the diffusive sublayer and due to the rough surface variations of the pressboard which are of the same order as the sublayer thickness.

Measurements will continue with new transformer oils and used oils taken from operating transformers. The equilibrium and energization models are also being improved by generalizing the electrochemical boundary condition at the interface to include chemical rate processes and moisture dynamics between pressboard and oil. Because of the bipolar nature of our measurements the charge transport model is also being extended to include

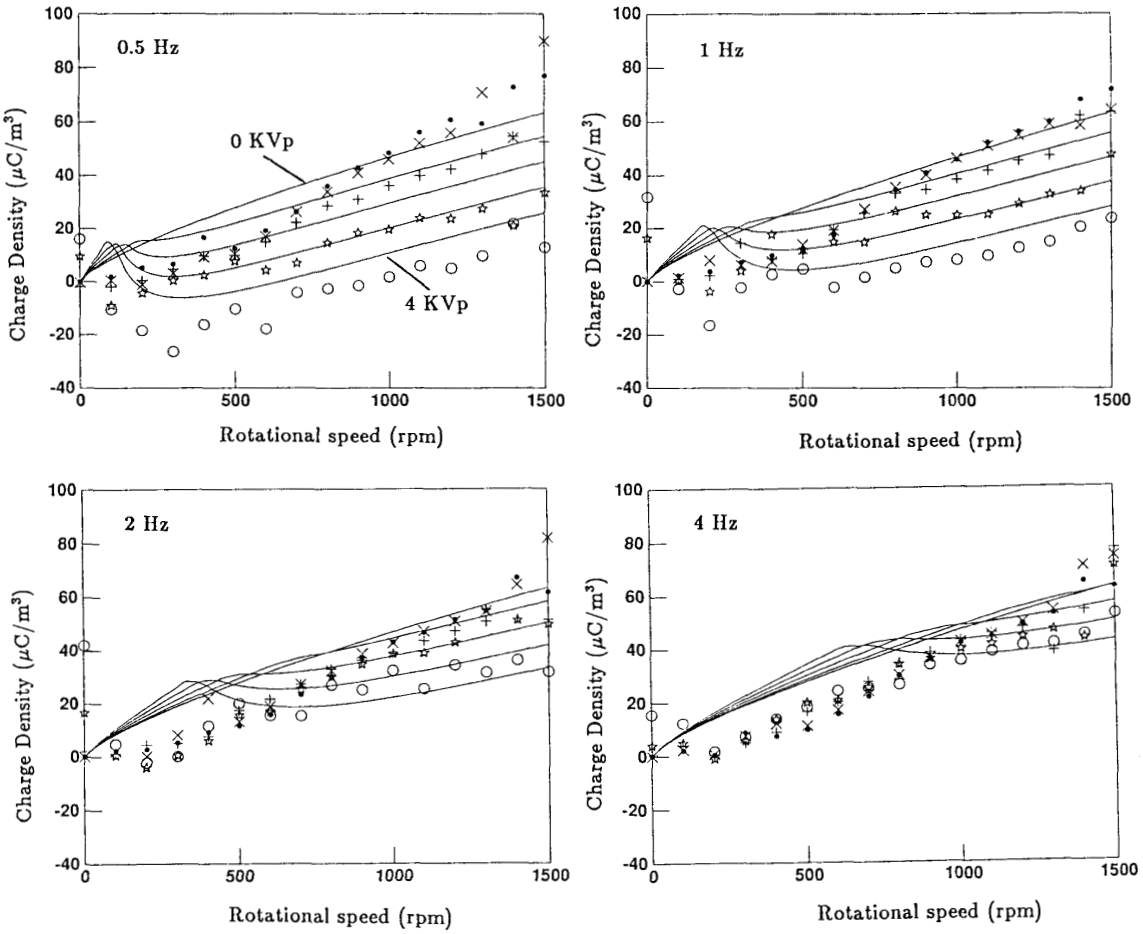

Figure 14.

Entry 6 of Table 6. Core charge density measured in the large CC with T–IV covered cylinders and Shell Diala A transformer oil at 2.7 ppm moisture with a dielectric relaxation time of 0.22 s. Data was taken at 70°C with $v = 0$ (dots) and with an applied ac voltage of 1 (crosses), 2 (pluses), 3 (stars), and 4 (circles) kV peak at 0.5, 1, 2, and 4 Hz with the rotational speed varied from 0 to 1500 rpm. The solid lines are calculated from (53) in the steady state using a three parameter best fit of $\rho_w = 20\,\mathrm{mC/m^3}$, $\rho_{inj} = -46\,\mathrm{mC/m^3}$, and $D = 2.83 \times 10^{-9}\,\mathrm{m^2/s} = 113\mathrm{D_m}$.

two opposite polarity charge carriers which are generated from dissociated neutral molecules with current due to migration in the electric field and by charge diffusion [58, 59]. Ion pairs can also recombine to reform neutrals, where in equilibrium the generation and recombination rates are equal. Such time and space dependent charge distributions are a better model of the conduction processes in highly insulating oils than the ohmic conductivity model generally used in this work.

ACKNOWLEDGMENT

THIS work was supported by the Electric Power Research Institute under Research Project 8000–31 under the management of Mr. S. R. Lindgren. Most of this work was part of A. J. Morin's thesis submitted to the M. I. T. Department of Electrical Engineering and Computer Science in partial fulfillment for the MS degree. Special thanks go to R. Albano for excellent machining of parts for the ACS and Couette Charger, D. Otten and T. Caloggero for design and construction of the circuitry

and mechanical components in the ACS, and W. Ryan, J. Kalt, P. von Guggenberg, A. Washabaugh, and P. Warren for help in taking and interpreting data.

REFERENCES

[1] A. Klinkenberg and J. L. Van der Minne, *Electrostatics in the Petroleum Industry*, Elsevier, Amsterdam, 1958.

[2] A. Klinkenberg, "Theoretical Aspects and Practical Implications of Static Electricity in the Petroleum Industry," in J. J. McKetta (ed.) *Advances in Petroleum Chemistry and Refining*, John Wiley and Sons, New York, Vol. 8, Chpt. 2, 1964.

[3] J. T. Leonard, "Generation of Electrostatic Charge in Fuel Handling Systems: A Literature Survey," NRL Report 8484, Sept., 1981.

[4] N. Denbow and A. W. Bright, "The Design and Performance of Novel On-line Electrostatic Charge-Density Monitors, Injectors, and Neutralizers for Use in Fuel Systems," in J. Lowell (ed.) *Electrostatics, 1979*, The Institute of Physics, London, pp. 171–179, 1979.

[5] I. Ginsburgh, "The Static Charge Reducer," J. Colloid Interface Sci., Vol. 32, pp. 424–432, 1970.

[6] A. Klinkenberg and B. V. Poulston, "Antistatic Additives in the Petroleum Industry," J. Inst. Petrol., Vol. 44, pp. 379–393, 1958.

[7] J. T. Leonard and H. F. Bogardus, "Pro-Static Agents in Jet Fuels," NRL Report 8021, August 1976.

[8] J. A. Carruthers and K. J. Marsh, "Charge Relaxation in Hydrocarbon Liquids Flowing Through Conducting and Non-Conducting Pipes," J. Inst. Petrol., Vol. 48, pp. 169–179, 1962.

[9] B. Abedian, "Electrostatic Charge Relaxation in Tank Filling Operations," J. Electrostatics, Vol. 14, pp. 35–57, 1983.

[10] K. Asano, "Electrostatic Potential and Field in a Cylindrical Tank Containing Charged Liquid," Proc. IEE, Vol. 124, pp. 1277–1281, 1977.

[11] J. A. Carruthers and K. J. Wigley, "The Estimate of Electrostatic Potentials, Fields, and Energies in a Rectangular Metal Tank Containing Charged Fuel," J. Inst. Petrol., Vol. 48, pp. 180–195, 1962.

[12] S. Yasufuku, J. Ise, Y. Inoue, and Y. Ishioka, "Electrokinetic Phenomena in Electrical Insulation Oil/Impregnated Cellulosic Pressboard System," IEEE International Symposium on Electrical Insulation, Paper No. E-4, 1967.

[13] T. Takagi, T. Ishii, T. Okada, K. Kurita, R. Tamura, and H. Murata, "Reliablity Improvement of 550 kV Large Capacity Power Transformer," CIGRE International Conference on large HV Electric Systems, Paper No. 12–02, August/Sept., 1978.

[14] M. Higaki, Y. Kako, M. Moriyama, M. Hirano, K. Hiraishi, and K. Kurita, "Static Electrification and Partial Discharges Caused Power Engineering Society Winter Meeting," Paper No. F79 231–2, New York, Feb., 1979.

[15] H. Okubo, M. Ikeda, M. Honda, and T. Yanari, "Charging Tendency Measurement of Transformer Oil," IEEE Power Engineering Society Winter Meeting, Paper No. A79051–4, New York, Feb., 1979.

[16] M. Higaki, H. Miyao, K. Endou, and H. Ohtani, "A Calculation of Potential Distribution Caused by Static Electrification Owing to Oil Flow in an Oil-Paper Insulation System and its Application to Partial Discharge Phenomena in Oil," IEEE Trans. Power App. and Sys., Vol. 98, No. 4, pp. 1250–1275, July/August, 1979.

[17] S. Shimizu, H. Murata, and M. Honda, "Electrostatics in Power Transformers," IEEE Trans. Power App., and Sys., Vol. 98, No. 4, pp. 1244–1250, July/August, 1979.

[18] H. Okubo, M. Ikeda, M. Honda, and S. Menju, "Electrostatic Discharges in Insulation Oil" International Symposium on HV Engineering, Paper No. 23.14, Milan, August, 1979.

[19] R. Tamura, Y. Miura, T. Watanabe, T. Ishii, N. Yamada, and T. Nitta, "Static Electrification by Forced Oil Flow in Large Power Transformers", IEEE Trans. Power App. and Sys., Vol. 99, No. 1, pp. 335–343, Jan./Feb., 1980.

[20] T. Tanaka, Y. Yasojima, N. Yamada, A. Kishi, and T. Nitta, "Model Approach to the Static Electrification Phenomena Induced by the Flow of Oil in Large Power Transformers", IEEE Trans. Power App. and Sys., Vol. 99, No. 3, pp. 1097–1106, May/June, 1980.

[21] M. Yasuda, K. Goto, H. Okubo, T. Ishii, E. Mori, and M. Masunaga, "Suppression of Static Electrification of Insulating Oil for Large Power Transformers", IEEE Power Engineering Society Winter Meeting, Paper No. 82 WM 197–2, New York, Jan./Feb., 1982.

[22] D. W. Crofts, "An Update of the Static Electrification Phenomena in Power Transformers", Presented to the Pennsylvania Electric Association, Hershey, PA, Sept. 16, 1985.

[23] D. W. Crofts, "Static Electrification Phenomena in Power Transformers", Special Session on Flow Electrification Effects in Electric Power Apparatus at the 1986 Conference on Electrical Insulation and Dielectric Phenomena, IEEE No. 86 CH2315-0, pp. 206–216, Nov.4, 1986.

[24] D. W. Crofts, "The Static Electrification Phenomena in Power Transformers", Special Issue on Flow Electrification in Electric Power Apparatus, IEEE Trans. Electrical Insulation, Vol. 23, No. 1, pp. 137–146, Feb., 1988.

[25] T. V. Oommen, "Static Electrification Properties of Transformer Oil", Special Session on Flow Electrification Effects in Electric Power Apparatus at the 1986 Conference on Electrical Insulation and Dielectric Phenomena, IEEE No. 86 CH2315-0, pp. 206–216, Nov.4, 1986.

[26] T. V. Oommen and E. M. Petrie, "Electrostatic Charging Tendency of Transformer Oils", IEEE Power Engineering Society Winter Meeting, Paper No. 84 WM164-0, Dallas, Jan./Feb., 1984.

[27] T. V. Oommen, "Static Electrification Properties of Transformer Oil", Special Issue on Flow Electrification in Electric Power Apparatus, IEEE Trans. Electrical Insulation, Vol. 23, No. 1, pp. 123–128, Feb., 1988.

[28] T. V. Oommen, "Static Electrification Control in Power Transformers", EPRI Final Report for RP 1499–7, Nov. 1987.

[29] E. Howells, M. Zahn, and S. R. Lindgren, "Static Electrification Effects In Transformer Oil Circulating Pumps", IEEE Trans. on Power Delivery, Vol. 5, No.2, pp. 1000–1006, April, 1990.

[30] S. M. Gasworth, J. R. Melcher, and M. Zahn, "Electrification Problems Resulting from Liquid Dielectric Flow", Technical Report EL-4501, EPRI, 1986.

[31] S. M. Gasworth, *Electrification by Liquid Dielectric Flow*, Ph. D. Thesis, Department of Electrical Engineering and Computer Science, MIT, Cambridge, MA, June, 1985.

[32] S. M. Gasworth, J. R. Melcher, and M. Zahn,"Flow-Induced Charge Accumulation In Thin Insulating Tubes", IEEE Transactions on Electrical Insulation, Vol. 23, No.1, pp. 103–115, Feb., 1988.

[33] J. K. Nelson,"The Use of a Tandem Chamber Charge Density Monitor In Transformer Applications", IEEE Transactions on Electrical Insulation, Vol. 25, No.2, pp. 399–404, 1990.

[34] J. R. Melcher, D. J. Lyon, and M. Zahn, "Flow Electrification in Transformer Oil/Cellulosic Systems", Special Session on Flow Electrification Effects in Electric Power Apparatus at the 1986 Conference on Electrical Insulation and Dielectric Phenomena, IEEE No. 86 CH2315-0, pp. 257–265, Nov.4, 1986.

[35] D. J. Lyon, J. R. Melcher, and M. Zahn, "Couette Charger for Measurement of Equilibrium and Energization Flow Electrification Parameters. Application to Transformer Insulation," Special Issue on Flow Electrification in Electric Power Apparatus, IEEE Trans. Electrical Insulation, Vol. 23, No. 1, pp. 159–176, Feb., 1988.

[36] D. J. Lyon, *Couette Flow Measurement of Equilibrium and Energization Charging in Transformer Insulation*, M. S. thesis, Dept. of Elect. Eng. and Comp. Sci., M. I. T., Cambridge, MA, July, 1987.

[37] J. R. Melcher, A. J. Morin II, and M. Zahn, An Instrument for the Detection of Electrical Charge Entrained in a Fluid U. S. Patent No.: 4, 873, 489, 1989.

[38] A. J. Morin II, J. R. Melcher, and M. Zahn, "An Absolute Charge Sensor for Fluid Electrification Measurements", Conference Record of the 1988 IEEE International Symposium on Electrical Insulation, pp. 18–22, June 5–8, 1988.

[39] A. J. Morin II, *Fluid Electrification Measurements of Transformer Pressboard/Oil Insulation In A Couette Charger Using An Absolute Charge Sensor*, M. S. thesis, Dept. of Elect. Eng. and Comp. Sci., M. I. T., Cambridge, MA, Sept. 1989.

[40] A. J. Morin II, M. Zahn, and J. R. Melcher, "Equilibrium Electrification Parameters Inferred from Couette Charger Terminal Measurements," Annual Report of the Conference on Electrical Insulation and Dielectric Phenomena, pp. 286–292, 1988.

[41] A. J. Morin II, M. Zahn, and J. R. Melcher, "Fluid Electrification Measurements in Transformer Pressboard/Oil Insulation", Conference Record of the 1989 International Symposium on HV Engineering, August/Sept., 1989.

[42] A. J. Morin II, M. Zahn, and J. R. Melcher, "Fluid Electrification Measurements of Transformer Pressboard/Oil Insulation In a Couette Charger Using An Absolute Charge Sensor", EPRI Technical Report EL-6918, Project 1499–98, Workshop Proceedings: Static Electrification in Power Transformers (Nov. 15–17, 1989, Princeton, NJ), pp. 3–3-1 to 3–3-33, July, 1990.

[43] A. J. Morin II, M. Zahn, J. R. Melcher, and D. Otten, "An Absolute Charge Sensor for Fluid Electrification Measurements", to be published, IEEE Transactions on Electrical Insulation, Vol. 26, pp. 181–199, 1991.

[44] I. Adamczewski, *Ionization, Conductivity and Breakdown in Dielectric Liquids*, Taylor and Francis, London, pp. 224–225, 1969.

[45] (a) F. M. White, *Fluid Mechanics*, McGraw-Hill, New York, Chapter 6, 1979; (b) *Viscous Fluid Flow*, McGraw-Hill, New York, pp. 423–426, 1974.

[46] A. S. Monin and A. M. Yaglom, *Statistical Fluid Mechanics*, Cambridge, MA, MIT Press, Vol. 1, Section 5.3, 1979.

[47] M. M. M. El Telbanny and A. J. Reynolds, "The Structure of Turbulent Plane Couette Flow", Trans. of the ASME Journal of Fluids Engineering, Vol. 104, pp. 367–372, Sept. 1982.

[48] A. A. Sonin, Notes from M. I. T. Course 2.273.

[49] B. Abedian and A. A. Sonin, "Theory for Electrical Charging in Turbulent Pipe Flow", J. Fluid Mech, Vol. 120, pp. 199–217, 1982.

[50] G. I. Taylor, "Fluid Friction Between Rotating Cylinders, Part I. Torque Measurements," Proc. Royal Society, Vol. CLVII, pp. 546–564, 1936.

[51] H. Schlicting, *Boundary-Layer Theory*, McGraw-Hill New York, chapter 20, 1979.

[52] B. Abedian, *Electric Charging of Low Conductivity Liquids in Turbulent Flows Through Pipes*, Ph. D. Thesis, Dept of Mechanical Engineering, M. I. T., Cambridge, MA., Sept. 1979.

[53] M. Ieda, K. Goto, H. Okubo, T. Miyamoto, H. Tsukioka, and Y. Kohno, "Suppression of Static Electrification of Insulating Oil for Large Power Transformers", Special Issue on Flow Electrification in Electric Power Apparatus, IEEE Trans. Electrical Insulation, Vol. 23, No. 1, pp. 153–157, Feb., 1988.

[54] M. C. Zaretsky, L. Mouayad, and J. R. Melcher, "Continuum Properties from Interdigital Electrode Dielectrometry", IEEE Transactions on Electrical Insulation, Vol. 23, No.6, pp. 897–917, Dec. 1988.

[55] H. G. Fischer, "Discussion to: Fluid Electrification Measurements of Transformer Pressboard/Oil Insulation In a Couette Charger Using An Absolute Charge Sensor", EPRI Technical Report EL-6918, Project 1499–98, Workshop Proceedings: Static Electrification in Power Transformers (Nov.15–17, 1989, Princeton, NJ), p. A-1, July, 1990.

[56] P. von Guggenberg and J. R. Melcher,"Moisture Dynamics in Paper/Oil Systems Subject to Thermal Transients," EPRI Technical Report EL-6918, Project 1499–98, Workshop Proceedings: Static Electrification in Power Transformers (Nov.15–17, 1989, Princeton, NJ), pp. 3–4-1 to 3–4-16, July, 1990.

[57] H. Miyao, M. Higaki, and Y. Kamata, "Influence of AC and dc Fields on Streaming Electrification of Transformer Oil," IEEE Trans. on Electrical Insulation, Vol. 23, No. 1, pp. 129–135, Feb., 1988.

[58] E. W. Jansen, *Bipolar Conduction Models for Dielectric Electrification*, M. S. Thesis, Dept. of Electrical Engineering and Computer Science, M. I. T., Cambridge, MA, Feb. 1990.

[59] E. W. Jansen and M. Zahn,"Drift/Diffusion Conduction Model for Flow Electrification", 1990 Conference on Electrical Insulation and Dielectric Phenomena, pp. 672–677, Oct. 1990.

Manuscript was received on 4 March 1991